THESIS FOR THE DEGREE OF LICENTIATE OF ENGINEERING

Characterization and Applications of Vector Phase-Sensitive Amplifiers

Abel Lorences-Riesgo

Photonics Laboratory
Department of Microtechnology and Nanoscience - MC2
CHALMERS UNIVERSITY OF TECHNOLOGY
Gothenburg, Sweden, 2015

Characterization and Applications of Vector Phase-Sensitive Amplifiers

Abel Lorences-Riesgo

Gothenburg, May 2015

ISSN 1652-0769
Technical Report MC2 - 308

Chalmers University of Technology
Department of Microtechnology and Nanoscience - MC2
Photonics Laboratory
SE-412 96 Gothenburg, Sweden
Phone: +46 (0) 31 772 1000

Printed by Bibliotekets reproservice, Chalmers University of Technology
Gothenburg, Sweden, May, 2015

Characterization and Applications of Vector Phase-Sensitive Amplifiers

Abel Lorences-Riesgo

Photonics Laboratory
Department of Microtechnology and Nanoscience - MC2
Chalmers University of Technology, SE-412 96 Gothenburg, Sweden

Abstract

This work is devoted to the characterization of vector phase-sensitive amplifiers and processors. A detailed analysis of degenerate vector phase-sensitive amplifier (PSA) is performed. The gain and phase-sensitive extinction ratio are theoretically analyzed using three-wave theory. Experiments and simulation results confirm the validity of this three-wave theory. The influence of polarization-mode dispersion is also evaluated, showing that aligning the pump polarizations at the fiber input is essential in order to achieve the theoretically predicted results. The scheme is also compared to the degenerate scalar PSA scheme. At the same pump power, the vector PSA has lower gain but also less influence from higher-order idlers and lower pump depletion due to four-wave mixing (FWM) between the pumps.

Using the degenerate vector PSA, phase-sensitive (PS) amplification of dual-polarization (DP) binary phase-shift keying (BPSK) signals was demonstrated. To the best of our knowledge, this was the first demonstration of a DP-modulated signal with large net phase-sensitive gain. Furthermore, we also demonstrated that this scheme can phase regenerate the signal. The same scheme was also used for a different purpose: quadrature decomposition into two cross-polarized waves. We demonstrated demultiplexing of quadrature phase-shift keying (QPSK) signal into two cross-polarized BPSK signals by the operating the amplifier in phase-insensitive mode. The design of a novel phase-locked loop scheme enabled stable operation and negligible penalty in the decomposition.

Keywords: fiber nonlinearities, four-wave mixing, parametric amplification, phase-sensitive amplification, all-optical processing

List of papers

Appended publications

This thesis is based on work contained in the following papers:

[A] **A. Lorences-Riesgo**, F. Chiarello, C. Lundström, M. Karlsson, and P. A. Andrekson, "Experimental analysis of degenerate vector phase-sensitive amplification", *Optics Express*, vol. 22, no. 18, pp. 21889–21902, Aug. 2014.

[B] **A. Lorences-Riesgo**, C. Lundström, F. Chiarello, M. Karlsson, and P. A. Andrekson, "Phase-sensitive amplification and regeneration of dual-polarization BPSK without polarization diversity", *in 2014 European Conference and Exhibition on Optical Communication (ECOC)*, Sept. 2014, paper Tu.1.4.3.

[C] **A. Lorences-Riesgo**, L. Liu, S. L. I. Olsson, R. Malik, A. Kumpera, C. Lundström, S. Radic, M. Karlsson, and P. A. Andrekson, "Quadrature demultiplexing using a degenerate vector parametric amplifier", *Optics Express*, vol. 22, no. 24, pp. 29424–29494, Nov. 2014.

Other publications

Related work by the author (not included in this thesis):

[D] C. Lundström, R. Malik, **A. Lorences-Riesgo**, Samuel L. I. Olsson, B. Corcoran, M. Karlsson, and P. A. Andrekson, "Fiber-optic Parametric Amplifiers Without Pump Dithering", *in Workshop on Specialty Optical Fibers and their Applications*, Aug. 2013, paper W3.12.

[F] **A. Lorences-Riesgo**, C. Lundström, M. Karlsson, and P. A. Andrekson, "Demonstration of degenerate vector phase-sensitive amplification", *in 39th European Conference and Exhibition on Optical Communication (ECOC)*, Sept. 2013, p. We.3.A.3.

[E] R. Malik, A. Kumpera, **A. Lorences-Riesgo**, P. A. Andrekson, and M. Karlsson, "Frequency-resolved noise figure measurements of phase (in) sensitive fiber optical parametric amplifiers", *Opt. Express*, vol. 22, no. 23, pp. 27821–27832, Nov. 2014.

[F] **A. Lorences-Riesgo**, T. A. Eriksson, C. Lundström, M. Karlsson, and P. A. Andrekson, "Phase-Sensitive Amplification of 28 GBaud DP-QPSK Signal", *in Optical Fiber Communications Conference (OFC)*, March 2015, paper W4C.4.

Acknowledgement

First, I would like to thank my supervisors Prof. Peter Andrekson and Prof. Magnus Karlsson for accepting me as a Ph. D. student. Their guidance and their support has been fundamental. Bill Corcoran also deserves my gratitude for the time he devoted to help me to put hands on experimental work. Thanks to Carl Lundström for sharing his knowledge about PSAs. Samuel Olsson also deserve special thanks for all the discussion about phase-sensitive amplifiers and about anything else such as vegetarian food. Not much helpful when coming to parametric amplification, Tobias Eriksson should be thanked for his help with coherent receivers, and for many ping pong games and football talks. Thanks to Rohit Malik and Aleš Kumpera for the fruitful PSA discussions.

Many thanks also go to two guest researches, Fabrizio Chiarello and Lan Liu, with whom I was fortunate to collaborate.

Thanks in general to all members of the Photonics Laboratory and FORCE group. I should especially mention Henrik Eliasson, thanks to who I got interested in green light and molecular symmetry.

Here, I also want to thank Prof. Christophe Peucheret who made me feel interested about fiber-optic communication in general.

Last but not least, I would like to thank my family and friends, especially my parents, my sister and of course Lara.

Abel Lorences-Riesgo

Gothenburg
May 2015

This work was financially supported by the European Research Council Advanced Grant PSOPA (291618). OFS Denmark and Sumitomo Electric Industries,

Ltd. are gratefully acknowledged for providing highly nonlinear fibers.

List of Acronyms

16QAM 16-ary quadrature-amplitude modulation

AQN amplified quantum noise
ASE amplified spontaneous emission
ASK amplitude-shift keying

BER bit-error rate
BPSK binary phase-shift keying

CW continuous wave

DGD differential group delay
DP dual-polarization
DSF dispersion-shifted fiber
DSP digital signal processing

EDFA erbium-doped fiber amplifier

FOPA fiber optical parametric amplifier
FWM four-wave mixing

GAWBS guided acoustic-wave Bragg scattering

HNLF highly-nonlinear fiber

NF noise figure
NLSE nonlinear Schrödinger equation

PBS polarization-beam splitter
PC polarization controller
PI phase-insensitive
PIA phase-insensitive amplifier
PLL phase-locked loop
PMD polarization-mode dispersion

PMF polarization-maintaining fiber
PPLN periodically-poled lithium niobate
PRBS pseudorandom bit sequence
PS phase-sensitive
PSA phase-sensitive amplifier
PSER phase-sensitive extinctio ratio
PSK phase-shift keying
PTN pump-transfered noise

QAM quadrature-amplitude modulation
QPSK quadrature phase-shift keying

RF radio frequency

SBS stimulated Brillouin scattering
SNR signal-to-noise ratio
SOA semiconductor optical amplifier
SOP state of polarization
SP single-polarization
SPM self-phase modulation
SRS stimulated Raman scattering
SSMF standard single-mode fiber

WDM wavelength-division multiplexing

XPM cross-phase modulation

ZDW zero-dispersion wavelength

Contents

Chapter 1

Introduction

During the last decades, fiber-optic communications systems have revolutionized the communication network by enabling large signal bandwidth and large transmission distances. Since the optical fiber was proposed in 1966 [1], fiber-optic communications systems have been evolving in order to meet the steadily increasing traffic demand. In this evolution, a key technology which significantly contributed to the capacity growth in fiber-optic communication system was the erbium-doped fiber amplifier (EDFA). Demonstrated in 1987 [2], the implementation of EDFAs in commercial systems in late 90s increased the traffic rate beyond 1 Tb/s. This increase highlights the importance of technologies for light amplification in today's optical network in which, despite the low loss of optical fibers (current record of 0.146 dB/km [3]), amplification is necessary after about 100 km of transmission. Apart from EDFAs, many other technologies have been proposed in order to perform light amplification, including semiconductor optical amplifiers (SOAs) [4, 5], Raman amplifiers [6, 7] and parametric amplifiers [8].

Among these amplifier technologies, parametric amplifiers have unique properties. Unlike EDFAs or other rare-earth doped amplifiers in which the bandwidth is dictated by the material, the bandwidth of a parametric amplifier can be tailored by designing the nonlinear medium. Gain bandwidth of about 155 nm with gain over 20 dB has been demonstrated [9]. Such a bandwidth is much higher than the typical EDFAs bandwidth of 35 nm. Moreover, 70 dB gain fiber optical parametric amplifier (FOPA) has been achieved [10]. An important property of parametric amplifiers is that they can be implemented in phase-sensitive (PS) mode, which means that the gain depends on the phases of the optical input waves. Phase-sensitive amplifiers (PSAs) are unique amplifiers since they can perform noiseless amplification. In contrast to phase-insensitive amplifiers (PIAs), such as EDFAs, SOAs, Raman amplifiers or parametric amplifiers operating in phase-insensitive (PI) moide, which have a quantum limited NF of 3 dB (assuming large gain), PSAs have a quantum-limited noise figure of 0 dB in the high-gain limit [11]. In other words, the signal-to-noise ratio (SNR) is not degraded in the case of PSAs whereas is halved in the case of PIAs. Such noiseless amplification is achieved by amplifying

correlated photons. In one-mode PSAs, one signal quadrature is amplified whereas the other quadrature is attenuated. In two-mode PSAs, amplification/attenuation is provided by the phase relation between the two non-degenerate input modes, known as the signal and the idler.

PSAs were experimentally demonstrated in second-order non-linear, χ^2, materials [12, 13] and third-order non-linear, $\chi^{(3)}$, materials [14] already in the 90s. Despite these demonstrations, not much attention was given to PSAs until about 10 years ago when the use of more advance modulation formats, the possibility to control the phase of the waves and the improvement in nonlinear fibers has made PSAs more practical, although still more complicated to implement than EDFAs or Raman amplifiers. In 2010, a PSA with 1.1 dB noise figure (NF) showed the potential of PSAs to perform low-noise amplification [15]. Such demonstration was performed in a two-mode PSA using the copier-PSA scheme [16], which is a modulation-format independent as well as a wavelength-division multiplexing (WDM) compatible scheme [17]. The benefit of low-noise amplification was also confirmed by demonstrating that the receiver sensitivity was improved by about 6 dB (3 dB when accounting for the idler power) when using a PSA-based receiver compared to an EDFA-based receiver in a back-to-back experiment with WDM signals [18] and in another experiment with single-channel single-span transmission [19]. As predicted theoretically [20, 21], the transmission distance in multi-span transmission in the linear regime is increased by a factor of four when using PSAs compared to EDFAs amplifiers [22]. In addition to performing low-noise amplification, PSAs can mitigate signal impairments caused by fiber non-linearities since idler and signal experience anti-correlated distortions [23]. Thus, the transmission distance is improved when operating in the linear regime as well as in the non-linear regime.

PSAs are also very attractive as regenerators since they squeeze the output signal phase. Moreover, amplitude regeneration can simultaneously be achieved by operating the amplifier in saturation. Then, PSAs can simultaneously regenerate the phase and the amplitude of noisy signals. PSAs performing all-optical regeneration were demonstrated using interferometric PSAs [24–26] and non-degenerate-pump PSAs [27]. In 2010, the demonstration of a black-box regenerator showed that PSA-based regenerators were practical and high performing [28]. Using binary phase-shift keying (BPSK) signals, increase of the transmission distance has been shown by implementing in-line regenerators in multi-span transmission [29]. Furthermore, the regeneration is not limited to BPSK signals and the regeneration of multilevel phase-shift keying (PSK) signals has also been demonstrated [30].

In addition to low-noise amplification and regeneration, all-optical functionalities such as quadrature demultiplexing [31–33] and [Paper C], and low-noise multi-casting [34] have been demonstrated using PSAs or phase-sensitive processors; showing the potential of using PSAs for all-optical processing. However, whereas optical networks encode data on two orthogonal polarizations, most work on PSAs has been performed using signals modulated in only one polarization.

Thus, further research on PSAs is needed in order to assess the possibilities of PSAs in dual-polarization (DP) scenarios.

1.1 This Work

This thesis is devoted to the experimental characterization and evaluation of vector PSAs which, as shown in the thesis, have the capability of PS amplification and regeneration of DP-modulated signals. In [Paper A], we characterize the performance of a degenerate vector PSA and compare to a degenerate scalar PSA. This analysis was the first demonstration of vector PSA with large gain. The gain and phase-sensitive extinctio ratio (PSER) were assessed as a function of the relative polarization angle between the signal and the idler. As predicted theoretically, the amplifier is not polarization-insensitive but has different potential applications including phase-to-polarization conversion, PS amplification of DP-BPSK signals and quadrature demultiplexing. The latter two applications were demonstrated in subsequent papers. In [Paper B], we demonstrate PS amplification of a DP-BPSK signal using a degenerate vector PSA. We also demonstrate that this scheme can perform phase-regeneration of both polarization channels, being the first demonstration of PSA-based regenerator of DP-modulated signals. In [Paper C], we demonstrate quadrature demultiplexing of a quadrature phase-shift keying (QPSK) signals into two cross-polarized waves by operating the degenerate vector amplifier in PI mode. A novel phase-locked loop (PLL) scheme is proposed and demonstrated to perform stable decomposition.

1.2 Thesis Outline

This thesis is organized as follows. In Chapter 2, we describe the wave propagation effects in optical fibers as well as how they relate to parametric amplification. Chapter 3 describes the process of parametric amplification. After explaining PI parametric amplification, we present the different schemes to achieve scalar and vector PS amplification. The chapter is concluded by highlighting the most promising applications of PSAs in conjunction with their main properties. Chapter 4 discusses both polarization-diverse and vector PSAs. We show that both schemes can phase-sensitively amplify DP-modulated signals. We conclude by pointing out different directions on PSA research in general, and more specifically on vector PSAs, in Chapter 5.

Chapter 2

Wave Propagation Effects

Both PS and PI parametric processors can be implemented in second-order, $\chi^{(2)}$, and third-order, $\chi^{(3)}$, nonlinear materials. For instance, bulk crystals [12, 13] and periodically-poled lithium niobate (PPLN) waveguides [35–37] have been used as $\chi^{(2)}$ platform for PS parametric processors. PS parametric processors based on third-order nonlinearities, $\chi^{(3)}$, materials, have been demonstrated using, e.g., silicon waveguides [38, 39], chalcogenide waveguides [40], lead-silicate-based highly-nonlinear fiber (HNLF) [41, 42], bismuth-oxide-based HNLF [43] and silica-based HNLF [15, 44]. Among all materials, silica-based HNLF is the medium in which the largest net parametric gain has been achieved. Moreover, it is the most compatible medium with the existing technology. For instance, it can be spliced to standard single-mode fiber (SSMF) with less than 0.3 dB loss, which is essential when targeting low NF. For these reasons, the nonlinear medium in which the lowest NF, 1.1 dB, with considerable net PS gain (>10 dB) has been achieved is also silica-based HNLFs as well [15].

Due to the aforementioned reasons, silica-based HNLFs is the nonlinear medium used in this thesis. In $\chi^{(3)}$ media such as HNLF, the desired nonlinearities to provide parametric effects are caused by the Kerr effect; the fiber refractive index dependence on the intensity of the optical field. Apart from the Kerr effect, FOPA features such as gain, bandwidth and NF are also determined by different linear and nonlinear effects. In order to gain understanding into parametric amplification, those effects of importance will be discussed in this chapter.

2.1 Linear Propagation Effects: Attenuation, Chromatic Dispersion and Birefringence

2.1.1 Fiber Attenuation

The fiber attenuation is mainly caused by material absorption and Rayleigh scattering. The attenuation in silica HNLFs is typically around 0.6-1.2 dB/km, which

is slightly higher than the attenuation in SSMF (0.2 dB/km). To account for the attenuation, the nonlinear effective length [45]

$$L_{\text{eff}} = \frac{1 - e^{-\alpha L}}{\alpha} \tag{2.1}$$

can be used instead of the physical fiber length L, where α is the attenuation in m^{-1}. In long fibers, we have $L_{\text{eff}} \approx \frac{1}{\alpha}$. In FOPAs, we often have $L_{\text{eff}} \sim L$ since short fibers (from 50 m to 1000 m) are usually preferred.

2.1.2 Chromatic Dispersion

The chromatic dispersion is the wavelength dependence of the speed of light, i.e., light at different wavelengths travels at different speed. To describe this effect, the propagation constant β is usually defined in a Taylor series around the center frequency ω_0

$$\beta = \beta_0 + \beta_1(\omega - \omega_0) + \frac{\beta_2}{2!}(\omega - \omega_0)^2 + \frac{\beta_3}{3!}(\omega - \omega_0)^3 + ..., \tag{2.2}$$

where $\beta_{\text{i}} = \frac{d^i \beta}{d\omega^i}\Big|_{\omega_0}$.

The phase velocity and group velocity are $v_{\text{p}} = \omega_0/\beta_0$ and $v_{\text{g}} = 1/\beta_1$ respectively. The second-order, β_2, and third-order, β_3, dispersion parameters determine the group-velocity dependence to the frequency. Instead of using frequency, describing the group-velocity dependence on the wavelength is often preferred. We then make use of the dispersion parameter, D, and the dispersion-slope parameter, S, which relate the group-velocity dependence on the wavelength, λ, as $D = \frac{dv_{\text{g}}}{d\lambda}$ and $S = \frac{dD}{d\lambda}$. The dispersion and the dispersion slope are related to the above Taylor expansion coefficients by

$$D = -\frac{2\pi c}{\lambda^2}\beta_2, \tag{2.3}$$

$$S = \left(\frac{2\pi c}{\lambda^2}\right)^2 \beta_3 + \frac{4\pi c}{\lambda^3}\beta_2, \tag{2.4}$$

where c is speed of the light in vacuum. In SSMFs, the dispersion and dispersion slope are $D \sim 16.5$ ps/(nm km) and $S \sim 0.09$ ps/(nm^2 km) at around $\lambda = 1550$ nm.

The fiber dispersion causes pulses to widen when they are travelling through the fiber. In FOPAs, dispersion and dispersion slope together with nonlinearities determine the gain and the bandwidth. As will be discussed in Section 3.1, the center wavelength of FOPAs is often in the anomalous regime ($D > 0$) but close to the zero-dispersion wavelength (ZDW). The fibers used in our experiments have a ZDW in the range from 1530 to 1575 nm, and a dispersion slope of about $S \sim 0.02$ ps/(nm^2 km). Though we have limited our analysis to dispersion and dispersion slope, higher-order dispersion parameters can be relevant in high-bandwidth FOPAs. Moreover, the dispersion fluctuations along the fiber also influence the performance of FOPAs [46–48].

2.1.3 Polarization-Mode Dispersion

The polarization-mode dispersion (PMD) is caused by fiber birefringence, i.e., waves with different polarizations do not experience the same refractive index due to fiber asymmetry caused by e.g., variation in the core shape, internal stress and external effects such as bends or lateral stress. Depending on the fiber design, fiber birefringence can be random or deterministic.

Polarization-maintaining fibers (PMFs) are fibers in which the birefringence is induced in the manufacturing process. Usually, a longitudinal stress is applied in the fiber, which causes a strong linear birefringence. By launching the input wave in one of the main axes (fast or slow axes), PMFs preserve the polarization of this wave through (ideally) infinite distances.

In optical fibers with random birefringence, the orientation of the main axes (locally defined fast and slow axes) changes randomly along the fiber. The length in which the main axes can be considered constant is only on the order of several meters. Moreover, fiber birefringence changes with time due to environmental changes such as vibrations, temperature and external stress. In these situations, the fiber PMD is a stochastic effect and it is usually analyzed in statistical terms. When a polarized continuous wave (CW) signal is launched into an optical fiber with random birefringence, its polarization will therefore change along the fiber. Moreover, the output polarization also depends on the signal wavelength. The two launched polarization states in which the output polarization is frequency independent to first-order approximation are the so-called principal states of polarization [49]. The difference in propagation time between a wave launched in one of the principal states of polarization compared to the wave launched in the other principal state of polarization is the differential group delay (DGD).

HNLFs can be either PMFs or fibers with random birefringence. Since polarization determines the strength of the nonlinearities, polarization-maintaining HNLFs would, in principle, be better than HNLF with random birefringence. However, manufacturing a polarization-maintaining-HNLFs with adequate values of dispersion and nonlinearities is challenging and expensive. Thus, and since lab-environments can be controlled, HNLFs with random birefringence are employed in most experiments. In scalar FOPAs, influence from fiber birefringence can be mitigated by launching the involved waves with principal state of polarizations (SOPs). However, PMD affects severely the performance of vector FOPAs [50,51], and more so when operating in PS mode [Paper A].

2.2 Kerr Effect

The refractive index of a material, n, does not only depends on the frequency but also on the intensity of the light, I. The effect of the refractive index dependence on the optical intensity is named the Kerr effect. When accounting for the Kerr

effect, the refractive index is usually expressed as [52]

$$n(\omega, I) = n_0(\omega) + n_2 I, \tag{2.5}$$

where $n_0(\omega)$ is the linear part and n_2 is the nonlinear refractive index. The nonlinear refractive index is related to the third order susceptibility, $\chi^{(3)}$, by

$$n_2 = \frac{3}{8n} Re(\chi^{(3)}), \tag{2.6}$$

where Re stands for the real part. Here, we have assumed that the light is linearly polarized, and $\chi^{(3)}$, which in general is a fourth-rank tensor, is expressed as a scalar. It is important to realize that the second-order susceptibility, $\chi^{(2)}$, vanishes in silica fibers due to molecular symmetry. Materials in which $\chi^{(2)}$ does not vanish can be used to achieve parametric amplification as well. In that case, amplification is based on second harmonic generation or sum- or difference-frequency generation.

In the analysis of wave propagation in fibers, the nonlinear coefficient, γ, is often used to incorporate the field distribution into the analysis since the intensity is determined by the field distribution. The nonlinear coefficient, γ, is defined as [45]

$$\gamma = \frac{2\pi n_2}{\lambda A_{\text{eff}}}, \tag{2.7}$$

where A_{eff} is the effective mode area, and thus it determines the confinement of the mode.

In order to analyze the nonlinear refraction with arbitrary SOPs, the 81 elements of the third order susceptibility tensor, $\chi^{(3)}$, should be considered. However, many of these elements vanishes due to symmetries and in the case of silica-based fiber there are only three independent terms [45, 52]. In addition, in the case of a random birefringent fiber, the analysis should ideally be performed in statistical terms. The analysis can be simplified by assuming that fiber birefringence does not change the relative polarization between the waves and that the SOP of the wave travelling through the fiber lies anywhere in the Poincaré sphere with equal probability. With these assumptions, the averaged coupled equations describing the field propagation are [53, 54]

$$i\frac{\partial A_{\text{u}}}{\partial z} + \frac{\beta_2}{2!}\frac{\partial^2 A_{\text{u}}}{\partial t^2} + \frac{\beta_3}{3!}\frac{\partial^3 A_{\text{u}}}{\partial t^3} + \gamma\left(|A_{\text{u}}|^2 + |A_{\text{v}}|^2\right)A_{\text{u}} = 0, \tag{2.8}$$

$$i\frac{\partial A_{\text{v}}}{\partial z} + \frac{\beta_2}{2!}\frac{\partial^2 A_{\text{v}}}{\partial t^2} + \frac{\beta_3}{3!}\frac{\partial^3 A_{\text{v}}}{\partial t^3} + \gamma\left(|A_{\text{v}}|^2 + |A_{\text{u}}|^2\right)A_{\text{v}} = 0, \tag{2.9}$$

where A_u and A_v are the wave components in two orthogonal polarizations. Here, γ has been reduced by 8/9 due to the PMD effects. This model, known as the Manakov model [55], provides insight in how the dispersion, the polarization and the nonlinearities interact. When one of the polarizations is neglected, the model corresponds to the well-known scalar nonlinear Schrödinger equation (NLSE). The

validity of the Manakov model depends on the considered bandwidth, fiber length and fiber birefringence. This model is not applicable when using short fibers, PMF fibers [45] or rapidly spun fibers [56]. Nor is it valid in cases where PMD is not negligible and changes the relative polarization between the waves. Considering the lengths of HNLFs employed in parametric amplification, the Manakov model is a reasonable assumption [45, 57] that significantly simplifies the analysis.

From the Manakov model, two important consequences are derived. First, the absolute polarization does not determine the strength of the nonlinearities. Second, the power in each polarization is conserved when neglecting the fiber loss.

2.2.1 Self-Phase Modulation

Self-phase modulation (SPM) is a process in which a wave propagating through the fiber phase modulates itself by inducing changes in the fiber refractive index. In the case of a CW, the nonlinear phase shift is described by

$$\Phi_{\mathrm{NL,SPM}} = \gamma P L_{\mathrm{eff}}, \tag{2.10}$$

where P is the power of the propagating wave. The interaction between dispersion and self phase modulation should be considered when analyzing propagation of pulses. An interesting effect of such interaction is the generation of optical solitons in which dispersion and nonlinearities cancel out [58, 59].

2.2.2 Cross-Phase Modulation

Cross-phase modulation (XPM) is a process in which two waves co-propagating through the fiber phase-modulate each other. The induced nonlinear phase shift on a CW by a second CW with power P_2 is

$$\Phi_{\mathrm{NL,XPM12}} = 2\gamma P_2 L_{\mathrm{eff}} \tag{2.11}$$

if we assume that both waves are co-polarized. Compared to SPM, XPM is twice as strong when both waves are co-polarized. However, XPM is an effect whose strength depends on the polarization of the involved waves. For example, the nonlinear phase shift is

$$\Phi_{\mathrm{NL,XPM12}} = \gamma P_2 L_{\mathrm{eff}} \tag{2.12}$$

when the two waves are cross-polarized (assuming the Manakov model). This means that the strength of XPM is half when having orthogonally polarized waves compared to parallel polarized waves.

Apart from polarization, dispersion should also be considered when accounting for the strength of cross-phase modulation. The walk-off length between pulses, i.e., the length in which pulses overlaps, may also limit the strength of the XPM-induced phase shift.

2.2.3 Four-Wave Mixing

Scalar Four-Wave Mixing

FWM, also named as four-photon mixing, is a process which involves the interaction between four photons and energy exchange between them. The energy exchange can be explained by the different gratings formed by the interference beating among waves at different frequencies. For instance, when two co-polarized waves, E_1 and E_2, with frequencies ω_1, ω_2 are co-propagating through the fiber, they generate an intensity beat tone with frequency $\omega_1 - \omega_2$. Thus, the fiber refractive index is modulated at this frequency in accordance with the Kerr effect. When a third wave, E_3 , also co-polarized and with frequency ω_3, also propagates together with the two previous waves, this third waves is phase modulated and new waves at frequencies $\omega_3 \pm (\omega_1 - \omega_2)$ are created [8]. In the same way, E_2 is modulated by the beating between E_1 and E_3 , and E_1 is modulated by the beating between E_2 and E_3. If all the waves have different frequencies, the FWM process is said to be non-degenerate. As shown in Figure 2.1, the non-degenerate FWM creates three new wavelengths at frequencies $\omega_{\mathrm{kmn}} = \omega_{\mathrm{k}} + \omega_{\mathrm{m}} - \omega_{\mathrm{n}}$ where $k, m, n \in \{1, 2, 3\}$, $k \neq m$, $k \neq n$ and $m \neq n$. Note that two terms are created at the same frequency. The degenerate processes include E_1 being modulated by the beating between itself and E_2 and the beating between between itself and E_3 ; and similarly to the cases in which E_2 and E_3 are modulated. The new frequencies created by degenerate processes are $\omega_{\mathrm{kmn}} = \omega_{\mathrm{k}} + \omega_{\mathrm{k}} - \omega_{\mathrm{m}}$ with $k, m \in \{1, 2, 3\}$, $k \neq m$. Six new frequency components are created when considering degenerate FWM. Taking into account degenerate and non-degenerate FWM, the total number of new frequency components is 9.

Vector Four-Wave Mixing

The previous explanation is valid for scalar FWM in which all waves are co-polarized. Vector FWM, in which waves have different polarizations can also occur. We now assume that two waves, E_1 and E_2, are co-polarized and a third wave, E_3, is cross-polarized with respect to them. In this case, the two co-propagating and co-polarized waves, E_1 and E_2, set the beat tone; and power from E_3 will be scattered to waves at frequencies $\omega_3 \pm (\omega_1 - \omega_2)$ as shown in Figure 2.2. These generated

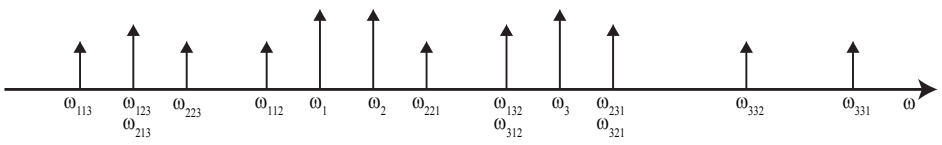

Figure 2.1: Schematic of waves generated by FWM processes when three input co-polarized waves are considered. The frequencies of the input waves are ω_1, ω_2 and ω_3.

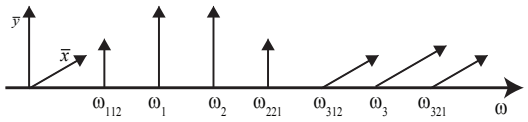

Figure 2.2: Schematic of waves generated by FWM processes when three input are considered, with two co-polarized waves and the third wave cross-polarized to them. The frequencies of the input waves are ω_1, ω_2 and ω_3.

waves are co-polarized with E_3. An special case is that in which $\omega_1 + \omega_3 = 2\omega_2$, and a new wave at the same frequency as E_2 but cross-polarized to E_2 is created. Combinations of E_1 -E_3 and E_2 -E_3 do not establish a intensity beat tone as they are cross-polarized pair of waves. The degenerate process involving E_1 and E_2 also generates new waves as explained previously with co-polarized waves.

Quantum-Mechanical Interpretion

From a quantum mechanical point of view, the FWM process is interpreted as follows: two photons at frequencies ω_1, ω_2 are annihilated, and two photons at frequencies ω_3 and ω_4 are created. FWM is a process in which energy is conserved, thus we have $\omega_1 + \omega_2 = \omega_3 + \omega_4$. Momentum is also conserved and establish the phase-matching condition which will be discussed in Section 3.1. Spin angular momentum is also conserved, determining the possible combinations of the spin of the annihilated photos and created photons. When the two annihilated photons have the same spin, the created photons also have the same spin as the annihilated photons. When the two annihilated photons have opposite spin, the two created photons also have opposite spin. As a consequence, power from two waves with right-hand circular polarization cannot scatter to two waves with right-hand circular polarization. However, power from two co-polarized waves with linear polarization can scatter to two waves with orthogonal polarization to the original wave. The latter case should be considered in short fibers. However, that case is not possible within the Manakov model.

In Chapter 3 we will provide more insight about the consequences of FWM and its use to achieve parametric amplification. We will also discuss the interplay between dispersion, SPM, XPM and FWM.

2.3 Raman Scattering

Raman scattering is an inelastic nonlinear process, caused by the imaginary part of the third-order susceptibility $\chi^{(3)}$. Raman scattering is commonly referred as the delayed response of the Kerr effect. From a quantum mechanical point of view, a photon is annihilated, and a photon at lower frequency is created as well as an optical phonon (vibration). The created downshifted photons can travel in

either forward direction or backward directions. In silica fibers, stimulated Raman scattering (SRS) gain has a large bandwidth with its peak being downshifted about 13.2 THz from the scattered wave [45]. Amplifiers using SRS are quite attractive since they can perform distributed amplification without the practical challenges of parametric amplifiers.

The effect of Raman scattering in parametric amplification can be either beneficial or detrimental. The SRS can be used to increase the FOPA gain and/or bandwidth [60]. However, Raman scattering affects the noise properties of parametric amplifiers, mainly in broadband parametric amplifiers [61, 62]. The NF degradation due to Raman scattering will be discussed in Section 3.5.

2.4 Brillouin Scattering

Brillouin scattering is an inelastic nonlinear process, caused by the electrostriction effect: the medium is compressed in presence of an optical field. As in the case of Raman scattering, Brillouin scattering involves energy transfer to the medium in form of an acoustic vibration. Contrary to SRS, the created downshifted wave only propagates backwards. The gain peak, dictated by the speed of the acoustic wave, is about 10 GHz in silica fibers, and the gain bandwidth is on the order of tens of MHz [45].

For narrow-band waves, stimulated Brillouin scattering (SBS) imposes a limitation on the maximum power that can be launched into the fiber [63]. This effect is then detrimental in parametric amplification in which the high-power pumps are commonly CWs. In order to overcome SBS, different techniques have been developed. The fiber can be doped with a material which lowers the SBS gain such as Al_2O_3 [64]. The use of these dopants to increase the SBS threshold do however increase fiber loss. Since the amplified wave travels backwards, the use of isolators is another way to mitigate SBS [65]. This technique cannot be however implemented in bidirectional parametric amplifiers. Furthermore, it also introduces additional losses. SBS is also reduced when the wave spectrum is broadened beyond the bandwidth of SBS [66]. In parametric amplification, the pump spectrum is usually broadened by phase modulation with radio frequency (RF) tones [67], white noise [68] or pseudorandom bit sequence (PRBS) [69]. However, the pump-phase modulation is transferred to the idler which is undesired when performing wavelength conversion. In PSAs, pump-phase modulation degrades the performance of the amplifier. In two-pump amplifiers, counter-phase modulation of the pumps can alleviate the penalty due to pump phase modulation [69]. Applying a temperature gradient [70,71] or strain gradient [72–74] in the fiber also decrease the SBS. As drawback, both temperature and strain causes ZDW fluctuations which might degrade the performance of parametric amplifiers [46]. The solution is applying the strain such that it mitigates inherent ZDW fluctuations of the HNLF as well as SBS [75]. Fiber straining also enhances the fiber PMD which is undesired in

parametric amplifiers [76]. Fiber more tolerant towards straining have been also designed [77]. These techniques can also be combined in order to achieve larger SBS suppression. For example, the combination of fiber straining and isolators has allowed to design parametric amplifiers with large net gain without pump spectral broadening [78].

SBS is often considered a detrimental effects on parametric amplification. However, it can also be used to enhance some FOPA properties. Using SBS to perform a phase shift on the signal can enhance FOPA bandwidth and gain [79–81]. In addition, such a method has also been shown to control the saturation characteristics in FOPAs [82]

Chapter 3

Fiber-Optic Parametric Amplification

In Chapter 2, we have discussed the wave propagation effects in optical fibers. In this chapter, we establish the connection between FWM and parametric amplification. We determine the input-output relations of FOPA and use these relations to discuss the different PSA schemes. The chapter is concluded by highlighting the main properties of PSA and their potential applications.

3.1 Phase-Insensitive Parametric Amplification

Parametric amplification can be achieved by means of both degenerate and non-degenerate FWM, and using either vector or scalar FWM. When using degenerate FWM in scalar PI-FOPAs, the input waves consists of a strong wave, known as pump, and a weak signal to be amplified. In this case, the most efficient process is the one in which power from the pump scatters due to the grating set by the pump and the signal. The pump power is indeed scattered to the signal wave and to a new wave, known as idler, at frequency $\omega_{\mathrm{I}} = 2\omega_{\mathrm{P}} - \omega_{\mathrm{S}}$ where ω_{P} and ω_{S} are the pump and the signal frequencies. The process in which power from the signal scatters can be usually neglected due to its lower strength. When using non-degenerate FWM in scalar PI-FOPAs, the input waves usually consists of two strong waves, pump waves, and the weak signal to be amplified. In vector PI-FOPAs, the input consists of two cross-polarized pumps and a signal. In both non-degenerate cases, the amplifier is often designed such that only one idler at frequency $\omega_{\mathrm{I}} = \omega_{\mathrm{P1}} + \omega_{\mathrm{P2}} - \omega_{\mathrm{S}}$ needs to be considered and other created waves can be neglected due to their lower strength. Here, ω_{P1} and ω_{P2} denote each pump frequency.

The evolution of the pumps, A_{P1} and A_{P2}, the signal A_{S} and idler, A_{I}, fields

can be described by a set of four coupled equations in both scalar and vector non-degenerate FWM processes. This set of four equations is obtained from applying Eqs. 2.8 and 2.9 to this situation. In scalar FWM, four co-polarized waves are considered. In the case of vector FWM, we assumed that both pumps are orthogonally polarized, which translates into a signal and idler which are also cross-polarized since spin number is also conserved. For simplicity, we assume that the signal field, A_{S}, is co-polarized with one pump, A_{P1}, and the idler field, A_{I}, is then co-polarized with the other pump, A_{P2}. Then, we have [83]

$$\begin{aligned}\frac{\partial A_{\mathrm{P1}}}{\partial z} =& i\gamma\left(|A_{\mathrm{P1}}|^2+\epsilon|A_{\mathrm{P2}}|^2+2|A_{\mathrm{S}}|^2+\epsilon|A_{\mathrm{I}}|^2\right)A_{\mathrm{P1}}\\ &+i\epsilon\gamma A_{\mathrm{S}}A_{\mathrm{I}}A_{\mathrm{P2}}^{*}\exp(i\Delta\beta z),\end{aligned} \tag{3.1}$$

$$\begin{aligned}\frac{\partial A_{\mathrm{S}}}{\partial z} =& i\gamma\left(|A_{\mathrm{S}}|^2+\epsilon|A_{\mathrm{P2}}|^2+\epsilon|A_{\mathrm{S}}|^2+2|A_{\mathrm{I}}|^2\right)A_{\mathrm{S}}\\ &+i\epsilon\gamma A_{\mathrm{S}}A_{\mathrm{I}}A_{\mathrm{P2}}^{*}\exp(-i\Delta\beta z),\end{aligned} \tag{3.2}$$

$$\begin{aligned}\frac{\partial A_{\mathrm{I}}}{\partial z} =& i\gamma\left(|A_{\mathrm{I}}|^2+\epsilon|A_{\mathrm{P1}}|^2+\epsilon|A_{\mathrm{S}}|^2+2|A_{\mathrm{P2}}|^2\right)A_{\mathrm{I}}\\ &+i\epsilon\gamma A_{\mathrm{S}}A_{\mathrm{I}}A_{\mathrm{P2}}^{*}\exp(-i\Delta\beta z),\end{aligned} \tag{3.3}$$

$$\begin{aligned}\frac{\partial A_{\mathrm{P2}}}{\partial z} =& i\gamma\left(|A_{\mathrm{P2}}|^2+\epsilon|A_{\mathrm{P1}}|^2+\epsilon|A_{\mathrm{S}}|^2+2|A_{\mathrm{I}}|^2\right)A_{\mathrm{P2}}\\ &+i\epsilon\gamma A_{\mathrm{S}}A_{\mathrm{I}}A_{\mathrm{P2}}^{*}exp(i\Delta\beta z),\end{aligned} \tag{3.4}$$

where the parameter $\epsilon = 2$ in the scalar cases and $\epsilon = 1$ in the vector case which allows the use of the same set of equations in both cases [83, 84]. The parameter $\Delta\beta = \beta_{\mathrm{S}} + \beta_{\mathrm{I}} - \beta_{\mathrm{P1}} - \beta_{\mathrm{P2}}\beta_{\mathrm{S}} - \beta_{\mathrm{I}}$ is the linear phase mismatch due to the difference of the pump, the signal and the idler propagation constants. These equations assume that the pumps, the signal and the idler are CW or negligible dispersion over the bandwidth of the signal, the idler and the pumps; and also negligible fiber loss. On the right-hand side, the different terms corresponding to SPM, XPM and FWM can be observed. The strength of XPM and FWM effects are halved when considering vector amplification. Here, we have used a set of four scalar equations, but a more general description in which the pumps can have any relative state of polarization is also possible when using Jones vectors [45]. By using the set of four scalar equations, we can gain much insight into the two most common cases in parametric amplification. In Chapter 4 Jones vectors will be used to generalize the vector PSAs for any arbitrary signal SOP.

Eq. 3.1 and 3.4 can be solved when the pumps remain undepleted. The pump fields are then given by [83]

$$A_{\mathrm{P1}} = A_{\mathrm{P1}}(0)\exp[i\gamma(P_{\mathrm{P1}} + \epsilon P_{\mathrm{P2}})L], \tag{3.5}$$

$$A_{\mathrm{P2}} = A_{\mathrm{P2}}(0)\exp[i\gamma(\epsilon P_{\mathrm{P1}} + P_{\mathrm{P2}})L], \tag{3.6}$$

where L is the fiber length, and the pump powers are denoted by $P_{\mathrm{P1}} = |A_{\mathrm{P1}}|^2$ and $P_{\mathrm{P2}} = |A_{\mathrm{P2}}|^2$. In the small-signal regime, the pumps are only affected by SPM and XPM between them. The solutions for the signal and the idler fields are then given by

$$\begin{aligned} A_{\mathrm{S}} = &[\mu A_{\mathrm{S}}(0) + \nu A_{\mathrm{I}}(0)^*] \\ &\cdot \exp(-i\beta L/2 + i\gamma\frac{3}{2}|A_{\mathrm{P1}}|^2 + i\gamma(\epsilon - 1/2)\frac{3}{2}|A_{\mathrm{P2}}|^2) \end{aligned} \tag{3.7}$$

$$\begin{aligned} A_{\mathrm{I}} = &[\mu A_{\mathrm{I}}(0) + \nu A_{\mathrm{S}}(0)^*] \\ &\cdot \exp(-i\beta L/2 + i\gamma\frac{3}{2}|A_{\mathrm{P2}}|^2 + i\gamma(\epsilon - 1/2)\frac{3}{2}|A_{\mathrm{P1}}|^2). \end{aligned} \tag{3.8}$$

In Eqs. 3.7 and 3.8, the phase term which affects equally both equations is often neglected for simplicity. The coefficients μ and ν defining the input-output relations are given by [83]

$$\mu = \cosh(gL) + i(\kappa/g)\sinh(gL), \tag{3.9}$$

$$\nu = i\epsilon\gamma(A_{\mathrm{P1}}A_{\mathrm{P2}}/g)\sinh(gL), \tag{3.10}$$

where $g = \sqrt{\epsilon^2\gamma^2 P_{\mathrm{P1}}P_{\mathrm{P2}} - (\kappa/2)^2}$ with $\kappa = \Delta\beta + \gamma(P_{\mathrm{P1}} + P_{\mathrm{P2}})$. The relation $|\mu|^2 - |\nu|^2 = 1$ is always fulfilled.

When both the signal and the idler are present at the fiber input, the signal gain depends on the relative phase between the optical waves. Such gain dependence on the phase relation between the input optical waves is what generates the so-called PS amplification. When there is no input idler, the amplifier is operating in the PI regime. The signal gain is in this case determined by

$$G = |\mu|^2 = 1 + \left(\frac{\epsilon\ \gamma(P_{\mathrm{P1}} + P_{\mathrm{P1}})}{g}\sinh(gL)\right)^2. \tag{3.11}$$

In this case, the idler is internally generated with a wavelength-conversion efficiency given by

$$|\nu|^2 = \left(\frac{\epsilon\ \gamma(P_{\mathrm{P1}} + P_{\mathrm{P1}})}{g}\sinh(gL)\right)^2. \tag{3.12}$$

Using Eq. 3.10 and assuming parametric gain, the phase of the generated idler, ϕ_{I}, is given by $\phi_{\mathrm{I}} = \pi/2 + \phi_{\mathrm{P1}} + \phi_{\mathrm{P2}} - \phi_{\mathrm{S}}$, where ϕ_{P1}, ϕ_{P2} and ϕ_{S} are the pump and signal phases respectively. As can be seen, the idler is a conjugated copy of the signal with an additional phase-shift.

The maximum gain will occur when g is maximized, i.e., $\kappa = 0$. This condition is known as the phase-matching condition. It states that the parametric gain is maximized when the linear phase shift and nonlinear phase shift cancel out. We

can also observe that phase-matching is obtained for both scalar and vector FWM with the same conditions. In other words, maximum parametric gain occurs for the same pump, signal and idler wavelength locations in both vector or scalar amplifiers. Assuming high gain, the gain when fulfilling phase-matching is given by

$$G = |\mu|^2 \approx exp[2L\epsilon\gamma\sqrt{(P_{\mathrm{P1}}P_{\mathrm{P2}})}]/4. \tag{3.13}$$

The gain has an exponential dependence on the pump power and the fiber length and fiber non-linear coefficient. For this reason, we commonly refer to this case as the exponential gain regime. Equation 3.13 also states that the scalar scheme has twice the gain in dBs than the vector scheme. However, in the scalar case, only the signal component parallel to the pump is amplified. In the vector scheme, both components are amplified. If the input signal is co-polarized to P_2, the same gain is easily obtained by exchanging the idler and signal in our previous analysis.

To gain insight in the gain bandwidth, we note that [45]

$$\Delta\beta = \beta_2 \left[(\omega_{\mathrm{S}} - \omega_{\mathrm{c}})^2 - \omega_{\mathrm{d}}^2\right], \tag{3.14}$$

where β is expanded around the center frequency $\omega_{\mathrm{c}} = \frac{\omega_{\mathrm{P1}}+\omega_{\mathrm{P2}}}{2}$ and we defined $\omega_{\mathrm{d}} = \frac{\omega_{\mathrm{P1}}-\omega_{\mathrm{P2}}}{2}$. The dispersion parameters β_4 and higher-order terms have been neglected. The third-order dispersion β_3 is considered but it does not determine $\Delta\beta$. Here, we can see that if the pumps are far apart, the second term in Eq. 3.14 dominates over a large bandwidth. In such a case, we desire $-\beta_2\omega_{\mathrm{d}}^2 = \gamma(P_{\mathrm{P1}} + P_{\mathrm{P2}})$ to achieve phase-matching. Then, we should be operating in the anomalous dispersion regime but close to the ZDW to achieve phase matching over a large wavelength range. This statement is valid for both two-pump scalar and vector parametric amplifiers. The gain bandwidth can be further increased at the expense of the gain peak by operating at the ZDW. In that case, β_4 should be considered as well in order to determine the gain bandwidth.

Here, we have limited our analysis to four-wave interaction. However, it is worth realizing that there are scenarios in which more waves needs to be considered. For instance, six waves should be considered in four-mode amplifiers in which there are three idlers to be considered [85]. We have also assumed that the pumps remain undepleted and thus, we are operating in the small-signal regime. The solution in the case of large signal power gain requires the use of elliptical functions [86]. The FWM between the pumps can also generate additional waves and deplete the pumps, invalidating this model.

The previous analysis is valid for non-degenerate FWM but it can be adapted to the different cases of degenerate FWM. The gain in the scalar pump-degenerate FWM can be calculated by assuming $A_{\mathrm{P1}} = A_{\mathrm{P2}} = A_{\mathrm{P}}/\sqrt{2}$ where A_{P} is the pump field. The bandwidth should be calculated by using $\Delta\beta = \beta_{\mathrm{S}} + \beta_{\mathrm{I}} - 2\beta_{\mathrm{P}}$, and therefore $\omega_{\mathrm{d}} = 0$. For this reason, achieving flat and large bandwidth in pump-degenerate schemes is not as simple as with dual-pump schemes. Assuming high gain, the gain has a quadratic dependence on the pump power when the

signal is located close to the pump wavelength [8]. The phase-matching condition, exponential regime, is only achieved for a certain signal-pump separation.

The scalar signal-degenerate FWM can be calculated by replacing $A_{\mathrm{I}} = A_{\mathrm{S}}$ in Eq. 3.7 and not considering Eq. 3.8. In the vector FWM, the signal-degenerate FWM can still be analyzed with the previous equations since signal and idler are two cross-polarized waves.

3.2 Scalar Phase-Sensitive Amplifiers

The four most common scalar PSA schemes are shown in Figure 3.1. If the signal and the idler are located at the same frequency, Figure 3.1 (top row), the amplifier is said to be one-mode amplifier. When the signal and the idler are located at two different frequencies, Figure 3.1 (bottom row), the amplifier is a two-mode amplifier. The cases of scalar one-mode and two-mode PSAs will be considered separately.

3.2.1 Scalar One-Mode Phase-Sensitive Amplifiers

The two most basic scalar one-mode PSA schemes are the fully-degenerate PSA and the signal-degenerate PSA. In the fully-degenerate PSA, Figure 3.1(a), the pump, the signal and the idler are located at the same frequency. In order to differentiate the signal from the pump, this scheme is implemented in an interferometer structure, either a Mach-Zehnder interferometer [14] or a Sagnac loop [87]. In the signal-degenerate PSA, Figure 3.1(b), the amplifier input waves are formed by the two pump waves, and the signal/idler wave. The frequencies of these waves are related by $2\omega_{\mathrm{S}} = \omega_{\mathrm{P1}} + \omega_{\mathrm{P2}}$.

In one-mode PSAs, the input-output relation is given by [14, 83]

$$S_{\mathrm{out}} = \mu S_{\mathrm{in}} + \nu S_{\mathrm{in}}^{*}, \tag{3.15}$$

where S_{in}, and S_{out} are the input and output signals. The parameters μ and ν are different to each case but they fulfill $|\mu|^2 - |\nu|^2 = 1$ regardless of the scheme. In the case of fully degenerate PSA, their values can be found by analyzing the non-linear phase-shift from SPM [88]. For the signal-degenerate PSA, we can calculate their values from Eqs. 3.9 and 3.10. The signal gain can be expressed as

$$G = \frac{|S_{\mathrm{out}}|^2}{|S_{\mathrm{in}}|^2} = |\mu|^2 + |\nu|^2 + 2|\mu||\nu| cos(\phi), \tag{3.16}$$

where $\phi = 2\phi_{\mathrm{S}} + \phi_{\mu} - \phi_{\nu}$; with ϕ_{S}, ϕ_{μ}, and ϕ_{ν} denoting the signal phase and the phases of the parameters μ and ν.

The gain dependence on the phase is shown in Figure 3.2. The maximum gain is

$$G_{\mathrm{max}} = \frac{|S_{\mathrm{out}}|^2}{|S_{\mathrm{in}}|^2} = |\mu|^2 + |\nu|^2 + 2|\mu||\nu| = (|\mu| + |\nu|)^2, \tag{3.17}$$

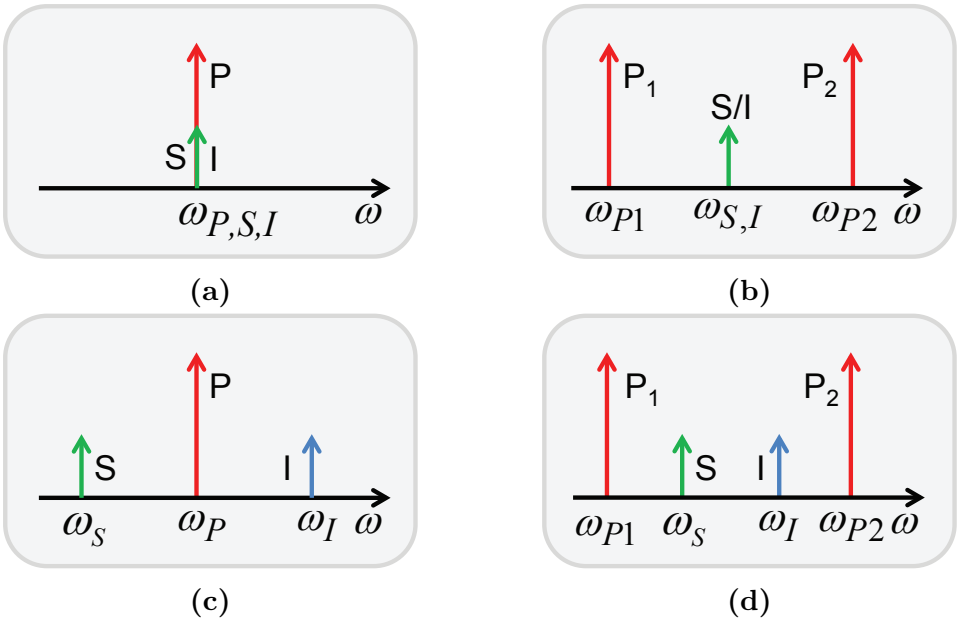

Figure 3.1: Scalar PSA schemes based on (a) fully-degenerate FWM, (b) signal-degenerate FWM, (c) pump-degenerate FWM and (d) non-degenerate FWM

and correspond to a signal with phase $\phi_S = \phi_\nu/2 - \phi_\mu/2$ or $\phi_S = \pi + \phi_\nu/2 - \phi_\mu/2$. The minimum gain or maximum attenuation is

$$G_{\min} = \frac{|S_{\text{out}}|^2}{|S_{\text{in}}|^2} = |\mu|^2 + |\nu|^2 - 2|\mu||\nu| = (|\mu| - |\nu|)^2, \tag{3.18}$$

corresponding to a signal with phase $\phi_S = \pi/2 + \phi_\nu/2 - \phi_\mu/2$ or $\phi_S = -\pi/2 + \phi_\nu/2 - \phi_\mu/2$. Obviously, $G_{\min}G_{\max} = 1$, which establishes that the maximum attenuation equals the maximum gain.

As can be seen from Equation 3.16, one-mode PSAs amplify one signal quadrature whereas the other quadrature component is attenuated, which means that the output signal phase is squeezed. In addition, the quadrature that is amplified can be selected by controlling the pump phases. Such effects has been utilized to achieve phase regeneration as will be discussed in Section 3.6.

Comparing the fully-degenerate PSA and the signal-degenerate PSA, the former one has several drawbacks. The gain dependence on the pump power is quadratic, contrary to all-other schemes here that under the phase-matching assumption have exponential dependence. The Mach-Zehnder interferometer is penalized by any mismatch between the two arms of the interferometer or between the couplers. The Sagnac loop non-linear interferometer is degraded by guided acoustic-wave Bragg scattering (GAWBS). Though 1.8 dB NF was demonstrated with such PSA, it was measured at 16 GHz [87] and at lower frequencies the performance was degraded by GAWBS.

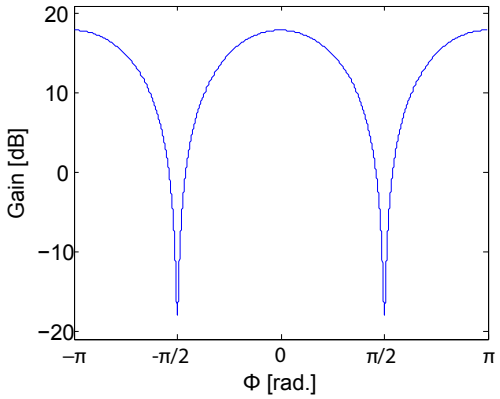

Figure 3.2: Gain vs. ϕ when the maximum PS gain is 18 dB

3.2.2 Scalar Two-Mode Phase-Sensitive Amplifiers

The pump-degenerate, Figure 3.1(c), and the non-degenerate PSAs, , Figure 3.1(d), are two-mode amplifiers since the interaction occurs between the signal and one idler which ar located at different frequencies. In the pump-degenerate PSA, the signal, the idler and the pump frequencies are related by $2\omega_{\mathrm{P}} = \omega_{\mathrm{S}} + \omega_{\mathrm{I}}$. In the non-degenerate PSA, we have $\omega_{\mathrm{P1}} + \omega_{\mathrm{P2}} = \omega_{\mathrm{S}} + \omega_{\mathrm{I}}$. The output signal, S_{out}, and idler, I_{out} are given by [20, 89]

$$\begin{bmatrix} S_{\mathrm{out}} \\ I^*_{\mathrm{out}} \end{bmatrix} = \begin{bmatrix} \mu & \nu \\ \mu^* & \nu^* \end{bmatrix} \begin{bmatrix} S_{\mathrm{in}} \\ I^*_{\mathrm{in}} \end{bmatrix}, \tag{3.19}$$

where S_{in} and I_{in} are the input signal and idler waves. The parameters μ and ν coefficients can be found from Eqs. 3.9 and 3.10 in the case of non-degenerate PSAs. We can also use these equations for the cases of pump-degenerate PSAs by replacing $A_{\mathrm{P1}} = A_{\mathrm{P2}} = A_{\mathrm{P}}/\sqrt{2}$ as already discussed. The signal gain can be expressed as

$$G = \frac{|S_{\mathrm{out}}|^2}{|S_{\mathrm{in}}|^2} = |\mu|^2 + |\nu|^2 + 2|\mu||\nu|\cos(\phi) \tag{3.20}$$

where $\phi = \phi_{\mathrm{S}} + \phi_{\mathrm{I}} + \phi_\mu - \phi_\nu$. We have have assumed that the signal and idler are equal in power, which translates into maximum PS interaction between both waves.

The maximum gain is given by Eq. 3.17 correspond to an idler which is a conjugated copy of the signal and an additional phase shift, $\phi_{\mathrm{I}} = -\phi_{\mathrm{S}} - \phi_\mu + \phi_\nu$. The minimum gain, given by Eq. 3.18, is also the inverse of the maximum gain in this case. We can also observe that the maximum gain corresponds to four times higher than the gain in phase-insensitive mode (Eq. 3.11), when assuming the high-gain regime ($\mu \sim \nu$).

The main difference of two-mode amplifiers with respect to one-mode amplifiers is that the former one can PS amplify any signal regardless of the modulation

format as long as the idler is a conjugated copy of the signal. In the degenerate case, only amplitude-shift keying (ASK) signals can be amplified.

3.3 Vector Phase-Sensitive Amplification

PS-FOPAs can be also be implemented in vector schemes. The two most basic schemes are the signal-degenerate vector PSA and the non-degenerate vector PSA, shown in Figure 3.3. As in vector PI-FOPAs, two orthogonal pumps are required and it is not possible to achieve vector PSA with a single-mode pump. It is worth realizing that we show the pump with linear SOPs, but this is not a requirement of vector schemes. Assuming the Manakov model, the pumps can take any SOP as long as they are cross-polarized. We here assume that the signal is co-polarized with P_1 for simplicity. Sections 4.5 and 4.4 cover the general case of any input signal and idler SOP. In the case of an input signal co-polarized to P_1, PS interaction occurs between a signal and an idler which are cross-polarized, as shown in Figure 3.3. Both schemes can be described as two-mode amplifiers since degenerate vector PSAs are degenerated in frequency but not in polarization; the signal and the idler have the same frequency but orthogonal polarizations. Similar to scalar PSAs, the frequencies of the waves fulfill $\omega_{\mathrm{P1}} + \omega_{\mathrm{P2}} = \omega_{\mathrm{S}} + \omega_{\mathrm{I}}$. The output signal, S_{out}, and idler, I_{out}, are determined by the same equations as two-mode amplifiers in scalars PSAs, Eq. 3.19. However, the parameters μ and ν take different values as discussed in Section 3.1. The signal gain is also defined as the signal gain in the scalar two-mode amplifiers, Eq. 3.20. As in scalar two-mode PSA, maximum amplification occurs when the signal and the idler are conjugated copies. The difference is that PS interaction occurs between two cross-polarized in the vector PSA.

Note that a degenerate vector PSA can also be described as a 1-mode vector PSA [90] when the signal and idler are equal in power and thus the degenerate wave, combination of signal and idler, forms a 45° angle (in Jones space) with both pumps. Under these assumptions, the degenerate vector PSA can be de-

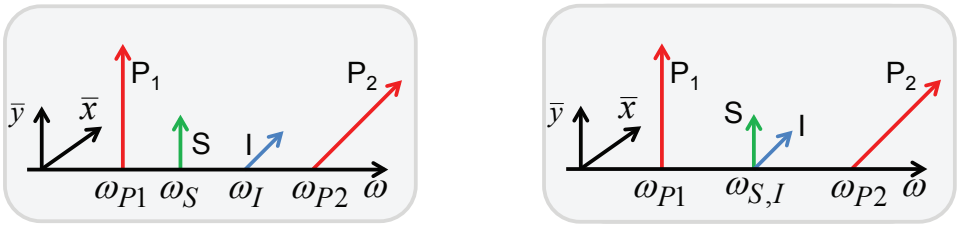

Figure 3.3: Vector PSA schemes based on (a) non-degenerate FWM and (b) signal-degenerate FWM

scribed by the input-output equation of 1-mode amplifier [90]. Such description of the degenerate-vector PSA is a particular case which does not provide a general description. The two-mode description of vector FWM is valid for any input polarization of the degenerate wave. It says that the process is PI when the input degenerate wave is aligned with one of the pumps and that maximum PS interaction occurs when the two signal components projected onto the two pump SOPs have equal power.

3.4 Phase-Sensitive Amplifiers in Transmission Systems

In all PSA configurations, the relative input phase relation among all waves, pump(s), signal and idler, determines whether the signal and idler are amplified or attenuated. Thus, pump, signal, and idler waves must be frequently and phase locked in order to achieve coherent amplification. If the signal, the idler and the pump(s) are not frequency and phase locked, amplification cannot be achieved. The generation of three/four phase and frequency locked waves can be implemented using a parametric amplifier operating in PI mode [16, 91], the so-called copier-PSA scheme. The illustration for the copier-PSA is shown in Figure 3.4(a). The copier generates the idler as a conjugated copy of the signal. The idler is located at frequency $\omega_{\mathrm{P1}} + \omega_{\mathrm{P2}} - \omega_{\mathrm{s}}$ and its phase is $\phi_{\mathrm{P1}} + \phi_{\mathrm{P2}} - \phi_{\mathrm{s}}$. Then, at the copier output, signal, idler and pump(s) are frequency and phase locked. In between the copier and the PSA, the mid-stage can vary in accordance with the application.

The mid-stage consisting of a filter with programable phase-response was used to characterize the PSA using CW in [92]. The dynamic response of the PSA can be measured by phase modulating some of the waves. For example, in experiments characterizing the pump-degenerate scalar PSA the pump(s), the signal and the idler were divided into two branches and only the pump was phase modulated [93, 94]. Note that modulating the three waves simultaneously would give an invariant relative phase. An important drawback when any of the waves travels through a different path is the need for a PLL which compensates for environmental drifts. Using signals modulated with data, differential PSA-based receivers have been demonstrated using a dispersive element as the mid-stage [95, 96]. The idler is delayed by one symbol period with respect to the signal in the dispersive element and in the PSA demodulation is achieved by beating of the idler and the signal. The mid-stage can also consist of a fiber link [19, 23] such that the PSA is placed at the receiver end to exploit the low-noise amplification provided by the PSA. As we will discuss in the next section, the copier-PSA scheme is the preferred option in transmission experiments since it is WDM-compatible and modulation format independent [15].

Modulation stripping has been proposed and demonstrated to operate as a

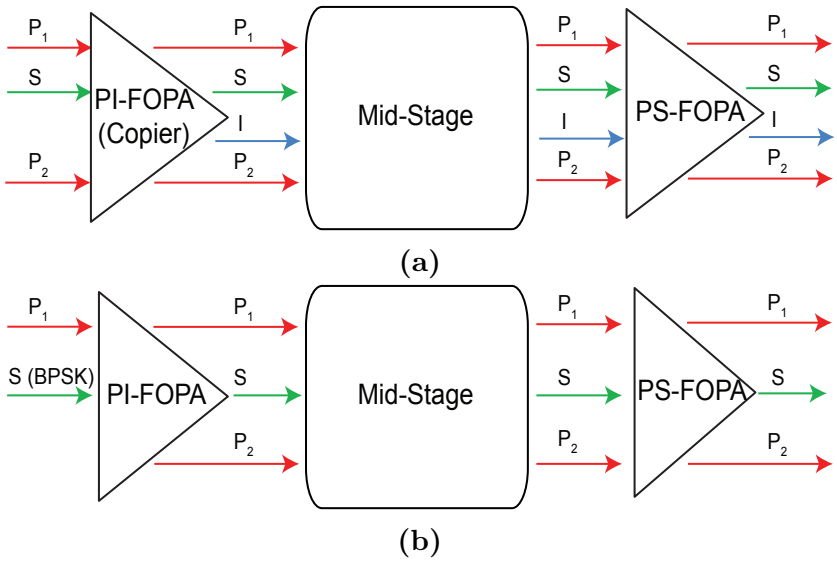

Figure 3.4: Schematic of (a) copier-PSA scheme (b) modulation stripping-PSA

pre-stage before the PSA [28, 44]. In its basic configuration, a CW and BPSK signal are combined in a parametric amplifier. The generated wave is located at the frequency $2\omega_s - \omega_{P1}$ and its phase is $2\phi_s - \phi_{P1}$. In other words, the second order harmonic of the BPSK signal has been generated. This harmonic corresponds to a CW since the phase modulation of the signal is erased. As will be discussed in Section 3.6, signal regeneration can be performed by implementing a signal-degenerate PSA after generating a modulation stripping pump.

Electro-optic combs have also been successfully proven in order to generate the corresponding phase and frequency locked waves before the PSA. Since no excess noise is added to the signal and idler as in the copier approach, the use of combs is of special interest when characterizing the PSA NF [97]. However, when requiring data-modulated signal and idler, with the idler being a conjugated copier of the signal, this scheme requires independent modulation of the signal and idler. A drawback of using the electro-optic comb is that the bandwidth of operation is limited by the bandwidth of the comb, usually hundreds of GHz.

3.5 Low-Noise Amplification

In our previous analysis, we have neglected the noise generated during the amplification process. The main contribution of noise in a parametric amplifier is the amplified quantum noise [62, 98, 99]. In a semi-classical analysis, we can calculate the output of a two-mode parametric amplifier as [15]

$$\begin{bmatrix} S_{out} \\ I^*_{out} \end{bmatrix} = \begin{bmatrix} \mu & \nu \\ \mu^* & \nu^* \end{bmatrix} \begin{bmatrix} S_{in} + n_S \\ I^*_{in} + n^*_I \end{bmatrix}, \tag{3.21}$$

where n_s and n_i represent the vacuum noise. They are statistically complex Gaussian distributions with $< n_{\mathrm{S,I}} >= 0$, $< n_{\mathrm{S,I}}^2 >= 0$ and $< |n_{\mathrm{S,I}}|^2 >= hf_{\mathrm{S,I}}/2$ where h is the Planck constant and f the optical frequency. Equation 3.21 is valid for the signal non-degenerate vector and scalar PSA.

In PI operation, assuming high gain and shot-noise limited input signal, the quantum-noise limited noise figure of a PI-FOPA is 3 dB [98]. Furthermore, the idler output noise is practically equal to the conjugated signal noise. From this fact, we know that detecting both signal and idler directly after the amplifier does not improve the SNR unless the detector is limited by thermal noise. We can also deduce that the quantum-limited noise figure of the wavelength conversion process is 3 dB.

When both input and signal idler are present at the input, we can also observe that the output noise does not vary. If the PSA is operating so that maximum gain is obtained, the output signal and idler powers are 6 dB higher than in the PI case, whereas the noise powers are the same. Therefore, the signal NF is -3 dB, 6 dB lower than the quantum-limited NF of a PI-FOPA. For the same reason, the quantum-limited idler NF is also -3 dB. The NF of the amplifier needs to take into account that both waves are present at the input, and it has been shown that it can be calculated as the sum of the idler and signal NF [15, 100]. Therefore, the quantum limited NF of PSAs is 0 dB which means that SNR is not degraded by the amplifier when assuming a shot-noise limited input. The unique property of performing noiseless amplification can only be possible in PSAs, i.e., amplifiers in which the gain depends on the phase of the input waves [11]. Here, it is important to realize that the NF is defined for a quantum-noise limited input, and therefore signal and idler noises are not correlated. If the idler is generated by the copier with high-gain, just after the copier the signal and idler noises are correlated. For that reason, loss in between the copier and the PSA is necessary in order to decorralate the signal and the idler noises and benefit from the low NF of PSAs.

The previous analysis regarding NF is valid for both scalar and vector PSAs as long as they can be defined as two-mode amplifiers. In the case of signal-degenerate scalar PSA, the quantum-limited NF is also 0 dB.

In the case of 4-mode PSAs, the quantum-limited NF is also 0 dB when four modes are present at the input. Therefore, when accounting for the noise performance, the use of 4-mode PSA is not practical due to the complexity increase of the 4-mode operation. It is important to realize that if in a 4-mode PSA, only two modes are present at the input, the noise figure will be degraded in accordance with the strength of the modes which are not at the input [84, 89]. For this reason, dual-pump parametric amplifiers are commonly designed such that only one idler is strong, so that the signal NF is not degraded.

Apart from amplified quantum noise (AQN), there are different noise contributions which degrade the performance of parametric amplifiers. These contributions are mainly the pump-transfered noise (PTN) [98] and Raman scattering [61]. PTN has its origin in the pump-power fluctuations. Since pumps are amplified by

EDFAs before being launched into the HNLF, the launched pumps have in-band amplified spontaneous emission (ASE) noise which cannot be filtered and cause power fluctuations. Since the gain depends on the pump powers, these power fluctuations are transferred as in-band noise to the signal and idlers. The performance degradation due to PTN has been analyzed both in PI-FOPAs [98, 99] and in PS-FOPAs [97]. Spontaneous Raman scattering also degrades the NF of FOPAs [61, 99, 101]. Raman-induced NF degradation impose an ultimate limit in order to experimentally achieve quantum-limited NF. For instance, it imposes a limit of 0.4 dB NF on the scalar pump-degenerate PSA [61]. However, despite the additional NF degradation effects, NF as low as 1.1 dB have been demonstrated in pump-degenerate PSA [15].

The capability of low-noise amplification makes PS-FOPA very promising as inline amplifiers and preamplifiers. In the back-to-back case or single-span links, 6 dB better sensitivity (3 dB when accounting for signal and idler power) is expected when using a PSA-base preamplifier compared to a PIA-based preamplifier due to the difference in the quantum-limited NF. This better sensitivity has been demonstrated using the copier-PSA scheme, with the copier at the transmitter and the PSA at the receiver in both back-to-back [18] and transmission implementations [19, 23]. In the latter case, the pump is attenuated before the link to avoid nonlinear effects within the link. At the receiver end, the pump is separated from the signal and idler. As we discussed, the pump needs to be recovered with fidelity such that PTN does not degrade the NF. In order to achieve such a pump recovery, the use of an optical injection-locking scheme has been proposed and demonstrated successfully [102]. In multi-span links, a scheme using the copier-PSA provides 4 times larger transmission distance (6 dB link NF improvement) when transmitting in the linear regime [20]. The 6 dB NF improvement comes from the 3 dB NF improvement of the PSA and from the fact that idler is considered as an internal mode. Such increase in transmission distance has recently been demonstrated in multi-span transmission with inline PS amplification. In all these demonstrations of PSA-amplified links, the PSA configuration was the scalar pump-degenerate PSA which simplifies the pump recovery. The use of pump-degenerate PSA in combination with the copier-PSA scheme translates into a scheme that is modulation format independent (as long as it is a single-polarization (SP) signal) and WDM compatible [15]. For instance, demonstration were performed with QPSK [103] and 16-quadrature-amplitude modulation (QAM) [23] signals. PS amplification of WDM signals has been demonstrated in a back-to-back scenario [18].

3.6 Phase Squeezing and Regeneration

PSAs have attracted much attention not only due to their low-noise amplification capabilities but also because the output phase is squeezed. Using the signal-degenerate scalar scheme, the output phase is squeezed to the real axis. When

operating in the linear regime, phase noise is converted into amplitude noise. Since the noise transformed, no major sensitivity improvement is expected [104]. If PSAs are operated in saturation, both amplitude and phase noise can be regenerated. Therefore, the scheme is suitable in order to achieve simultaneous phase and amplitude regeneration of BPSK signals. A requirement in order to have such a scheme is the presence of two pumps located symmetrically around the signal. Furthermore, the generation of such pumps must be performed in a black-box implementation, meaning that the input consists of only the modulated signal. In order to achieve such a black-box implementation, modulation stripping and the use of a injection-locking laser has been proposed and successfully demonstrated [28, 44, 104, 105]. Modulation stripping is achieved by combining a pump wave with the signal and mixing in a parametric amplifier as shown in Figure 3.4(b). In order to simultaneously amplify and filter the second-harmonic of the signal, an injection-locked laser is used. After this process, the two pumps (symmetrically located around the signal) and the signal are input into the degenerate-signal PSA. After the PSA, the signal phase and amplitude are regenerated when operating in saturation.

The concept has also been extended to perform regeneration of m-PSK signals [30,106]. In order to regenerate a m-PSK signal, the signal must be coherently added with its (m-1)$^{\text{th}}$ conjugated harmonic. The black-box regenerator consists of two stages, a first PI stage in which the (m-1)$^{\text{th}}$ and the m$^{\text{th}}$ harmonics are generated by cascaded FWM. Note that modulation stripping is achieved in the m$^{\text{th}}$ conjugated harmonic. In second stage, the harmonic wave and the signal are combined by means of a non-degenerate scalar PSA. It has been also demonstrated that the presence of (m-1)$^{\text{th}}$ conjugated harmonic wave at the input of the second stage is not necessary because it is internally generated as the PSA is operated in saturation [107]. Moreover, operation in saturation also provides amplitude regeneration.

There have been also demonstrations including regeneration of m-QAM signals such as 8-QAM [108]. However, regeneration of multilevel signals is hindered by the lack of schemes to amplitude regenerate multilevel signals. Regeneration of 16-ary quadrature-amplitude modulation (16QAM) signals can be achieved by the regeneration of inner and outer QPSK signals into which the 16QAM signal can be divided [109].

Another application in which phase-squeezing is desired is quadrature demultiplexing [33]. When the input signal is modulated in both quadratures, e. g. QPSK signals, only one quadrature will be output by the PSA when assuming high-gain. The additional quadrature can be obtained by a second PSA. Quadrature demultiplexing can also be achieved with a degenerate vector parametric amplifier operating on phase-insensitive mode [Paper C]. Such scheme will be discussed in Section 4.5.

3.7 All-Optical Mitigation of Fiber Nonlinearities

PSAs can also mitigate the effect of fiber nonlinearities on modulated signals [22, 23,103,110]. The explanation of such mitigation is that when transmitting two conjugated signals in two orthogonal dimensions, they will experience anticorrelated nonlinear phase shift when the dispersion map is symmetric [111]. The technique of transmitting two conjugated copies is known as the twin-wave concept. In the case of a PSA-amplified link, the idler and the signal are transmitted through the link after being generated by a copier. Using perturbation analysis, the signal and idler fields after the link, S_{L} and I_{L}, can be expressed as [111]

$$S_{\mathrm{L}} = S_0 + \delta E \tag{3.22}$$

$$I_{\mathrm{L}} = I_0 - \delta E^* \tag{3.23}$$

where the dispersion and the power maps are considered to be symmetric, and S_0 and I_0 are the signal and idler at the link input. The distortions introduced by the nonlinearities during transmission are defined by δE. It is clear from Eqs. 3.22 and 3.23 and the input-output relations, Eq. 3.19, that PSAs cancel the distortions due to fiber nonlinearities under such assumptions.

Nonlinear effects can also be suppressed by digital coherent superposition [111–113]. A comparison between PSA-based and digital-based mitigation has shown that both techniques perform similarly [114]. In terms of practical implementation, the PSA requires optical dispersion compensation whereas when using digital signal processing (DSP), dispersion can be compensated digitally.

Chapter 4

Phase-Sensitive Amplification of Dual-Polarization Signals

As we have seen in Chapter 3, PSAs are promising to perform functionalities such as low-noise amplification, regeneration and mitigation of fiber nonlinearities among many applications. However, most experimental demonstrations have been performed with data encoded in one polarization whereas optical networks often encode data using both polarizations. Thus, demonstrations of PSAs compatible with DP signals are necessary in order to show the full potential of PSAs. For PI-FOPAs, two different solutions were demonstrated to achieve polarization-independent performance: polarization-diversity [115–118] and vector schemes [119–121]. This thesis is devoted to the characterization of vector PS-FOPAs and its applications. In this context, the comparison between vector and polarization diverse PSAs is necessary. To do such a comparison, we analyze if polarization-independent PS-FOPAs can be obtained by implementing either polarization-diverse PSAs or vector PSAs. Our analysis is performed using the Jones description of both the polarization-diverse and the vector schemes in conjunction with the input-output description of PSAs. We conclude this chapter by comparing both schemes in practical terms.

4.1 Polarization-Diverse Implementations

Scalar PSAs only amplifies one polarization and polarization diversity is needed to amplify both polarizations. Such a polarization-diverse PSA [37,122] is usually implemented in a loop similar to polarization-diverse PI-FOPAs [115–118]. Figure 4.1 shows two possible implementations of polarization-diverse FOPAs. The pumps, or pump in case of pump degenerate FWM, have linear polarization at 45° so that their power is equally divided after the polarization-beam splitter (PBS). In the case of signal-degenerate FWM, the input waves are the pumps and the signal. In this scheme, a polarization controller (PC) is used to direct the output to the other

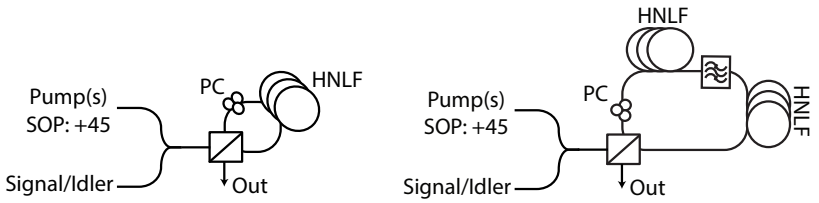

Figure 4.1: Polarization-diversity FOPA implemented in a loop with (a) one nonlinear medium (b) two nonlinear media and filter removing the pumps.

port by compensating for polarization rotations within the fiber. By using a loop, both signal components are combined coherently after being amplified as shown Figure 4.1(a). When using the loop implementation, the same nonlinear medium can be used to amplify both signal components. However, degradation of the amplifier performance has been already reported in bidirectional PI-FOPAs [118,123], caused by Rayleigh and Brillouin scattering. This degradation is expected to be detrimental when requiring low-noise PS amplification. It can be mitigated by implementing a loop with two different nonlinear media, as shown in Figure 4.1(b). A similar scheme has already been experimentally demonstrated using $\chi^{(2)}$-material-based PSAs [122]. As can be seen, the pumps are attenuated by e.g. an optical filter in between the two FOPAs. Then, the amplification of each polarization component occurs in each HNLF.

4.2 Polarization-Diverse Two-Mode Phase Sensitive Amplification

When implementing a polarization-diversity scheme, the output signal and idler (non-degenerate signal) are determined by [90]

$$S_{\text{out}} = \mu S_{\text{in}} + \nu I_{\text{in}}^{*}, \tag{4.1}$$

$$I_{\text{out}} = \mu I_{\text{in}} + \nu S_{\text{in}}^{*}, \tag{4.2}$$

where S and I correspond to the signal and idler Jones vectors. The operator $*$ denotes conjugation in each vector component. The matrix coefficients μ and ν were defined in Eqs. 3.9 and 3.10 for the non-degenerate and the pump-degenerate FOPAs. We have assumed that the phase relation at the input of both amplifiers is not affected by dispersive elements between the PBS and both amplifier inputs. We have also assumed that both FOPAs perform equally. In practical terms, the same gain is achieved by using the same HNLF in bidirectional implementation [124], but the NF can vary due to ZDW fluctuations [48]. When using two nonlinear

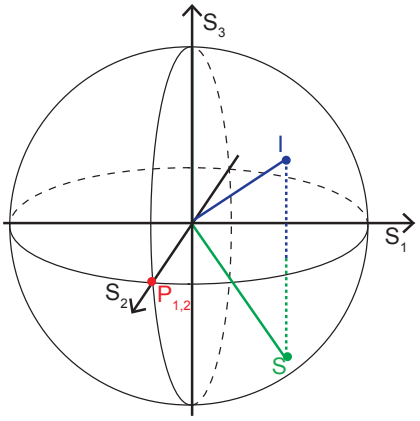

Figure 4.2: Relation between signal and idler SOPs to achieve maximum PS interaction in polarization-diverse PSAs. The idler SOP is a mirror of the signal SOP with the mirror plane defined by $S_3 = 0$.

media, the gain must be equalized for both FOPAs, which can be challenging in the case of broadband amplification since it requires identical HNLFs.

The gain dependence on the polarizations and phases of the signal and idler is given by

$$\begin{aligned} G =& \frac{|S_{\text{out}}|^2}{|S_{\text{in}}|^2} = |\mu|^2 + |\nu|^2 \\ &+2|\mu||\nu|[\cos(\theta_{\text{S}})\cos(\theta_{\text{I}})\cos(\phi_{\text{S}} + \phi_{\text{I}} + \varphi_{\text{S}}/2 + \varphi_{\text{I}}/2) \\ &+\sin(\theta_{\text{S}})\sin(\theta_{\text{I}})\cos(\phi_{\text{S}} + \phi_{\text{I}} - \varphi_{\text{S}}/2 - \varphi_{\text{I}}/2)], \end{aligned} \tag{4.3}$$

where we defined

$$S_{\text{in}} = |S_{\text{in}}|e^{i\phi_{\text{S}}} \begin{bmatrix} \cos(\theta_{\text{S}})e^{i\varphi_{\text{S}}/2} \\ \sin(\theta_{\text{S}})e^{-i\varphi_{\text{S}}/2} \end{bmatrix}, \tag{4.4}$$

$$I_{\text{in}} = |I_{\text{in}}|e^{i\phi_{\text{I}}} \begin{bmatrix} \cos(\theta_{\text{I}})e^{i\varphi_{\text{I}}/2} \\ \sin(\theta_{\text{I}})e^{-i\varphi_{\text{I}}/2} \end{bmatrix}, \tag{4.5}$$

where ϕ_{S} defines the signal global phase, φ_{I} defines the phase relation between signal polarization components and θ_{I} determines the magnitude of the wave in each polarization component. We have assumed equal input signal and idler powers, $|S_{\text{in}}|^2 = |I_{\text{in}}|^2$. To simplify the analysis, we have also assumed that μ and ν are real which can be achieved by tuning the pump phases and perfect phase-matching.

From Eq. 4.3, we can observe that maximum amplification can only be achieved when the signal and idler SOPs fulfill $J_{\text{S}} = J_{\text{I}}^*$ $\theta_{\text{S}} = \theta_{\text{I}}$ and $\varphi_{\text{S}} = -\varphi_{\text{I}}$, and the idler is a conjugated copy of the signal, $\phi_{\text{S}} = -\phi_{\text{I}}$. Using the conversion between Jones vector and Stokes vector presented in the Appendix, we can observe that maximum

PS amplification can only be achieved when the idler polarization (described with Stokes parameters) fulfills

$$I_{\text{in}} = \begin{bmatrix} I_1 \\ I_2 \\ I_3 \end{bmatrix} = \begin{bmatrix} S_1 \\ S_2 \\ -S_3 \end{bmatrix}, \tag{4.6}$$

where $S_{\text{in}} = \begin{bmatrix} S_1 \\ S_2 \\ S_3 \end{bmatrix}$ describes the signal input polarization using Stokes description. Figure 4.2 shows this relation between the signal and the idler polarizations to achieve maximum PS interaction using the Poincaré sphere. Maximum PS interaction occurs e.g., when the idler SOP is a mirror image of the signal SOP in the $S_3 = 0$ plane. Maximum gain can be obtained for e.g. when the signal and idler are both co-polarized with linear polarization. If signal and idler are cross-polarized with circular SOP, $\theta_{\text{S}} = \theta_{\text{I}} = \pi/4$ and $\varphi_{\text{S}} = \varphi_{\text{I}} = \pi/2$, maximum gain can be also obtained. On the other hand, if the signal and idler are cross-polarized with linear SOP, $\theta_{\text{S}} - \pi/2 = \theta_{\text{I}}$ and $\varphi_{\text{S}} = \varphi_{\text{I}} = 0$, the output signal and idler powers do not depend on the phase of the input waves. Such PI gain is also obtained if the signal and idler are co-polarized with either right of left hand circular polarization. Therefore, the maximum gain depends on the relative SOP between the signal and the idler as well as on their absolute SOP.

An idler which fulfills the conditions to achieve maximum amplification can be generated by a polarization-diverse PI-FOPA, without any constraint in the input signal to the copier. Thus, PS amplification of DP-modulated signals can be achieved by the means of copier-PSA with polarization-diversity. However, the implementation of the copier-PSA with a polarization-diverse PSA will be affected by any absolute change of polarization in either the signal, the idler or both during the mid-stage. In other words, first-order PMD will affect the performance of the scheme [90]. For instance, if the copier generates a signal and idler which are co-polarized with linear polarization; and in the mid-stage their polarization is rotated to circular polarization, it will not be possible to achieve maximum amplification in the PSA.

4.3 Polarization-Diverse One-Mode Phase Sensitive Amplification

The signal-degenerate case can be analyzed by substituting I_{in} by S_{in} in Eq. 4.1 which gives

$$S_{\text{out}} = \mu S_{\text{in}} + \nu S_{\text{in}}^{*}. \tag{4.7}$$

In this case, the gain is determined by

$$G = \frac{|S_{\text{out}}|^2}{|S_{\text{in}}|^2} = \\ |\mu|^2 + |\nu|^2 + 2|\mu||\nu|[\cos^2(\theta_{\text{S}})\cos(2\phi_{\text{s}} + \varphi_{\text{S}}) + \\ \sin^2(\theta_{\text{S}})\cos(2\phi_{\text{S}} - \varphi_{\text{S}})] \tag{4.8}$$

where the signal is defined as in Eq. 4.4, and we assume, as in the previous section, that μ and ν are real. We will consider the cases of PI and PS gain separately.

4.3.1 Phase-Insensitive Gain

From Eq. 4.8, we realize that if the input signal is circularly polarized, $\theta_{\text{S}} = \pi/4$ rad and $\varphi_{\text{S}} = \pi/2$ rad, the gain

$$G = |\mu|^2 + |\nu|^2 \tag{4.9}$$

does not depend on the signal phase. In this case, phase-to-polarization conversion is performed since the ratio between the output $'x'$ and $'y'$ components depends on the signal input phase. Assuming high-gain ($|\mu| \sim |\nu|$), we have

$$S_{\text{out,x}}/S_{\text{out,y}} \sim \tan^{-1}(\phi_{\text{S}} + \pi/4). \tag{4.10}$$

which indicates that when the relation between both polarization components is determined by the signal input phase.

The previous equation states that quadrature demultiplexing into two cross-polarized waves can be performed with this scheme when the input signal is circularly polarized. When assuming high gain, the in-phase component is projected on the output component with at +45° linear polarization and the quadrature component on the wave component with -45° linear polarization.

4.3.2 Phase-Sensitive Gain

Looking at Eq. 4.8, we can observe that both 'x' and 'y' components are simultaneously PS amplified with maximum gain when they have the same phase, i.e., the input signal is linearly polarized. The gain in the case of an input signal with linear SOP, $\varphi_{\text{S}} = 0$, is

$$G = |\mu|^2 + |\nu|^2 + 2|\mu||\nu|\cos(2\phi_{\text{s}}). \tag{4.11}$$

Therefore, all signal instantaneous SOPs are amplified for the same relative phase between the signal and the pumps. The relation between both polarization output components

$$S_{\text{out,x}}/S_{\text{out,y}} = \tan^{-1}(\theta_{\text{S}}) \tag{4.12}$$

is the same as this relation at the input, which means that the signal polarization is maintained.

The scheme can therefore phase-sensitively amplify all modulation symbols of a DP-ASK signal in which the polarization channels are linear and both polarization channels are modulated in the in-phase component. Furthermore, the output phase is squeezed for both polarization channels when assuming high gain which means phase regeneration is performed in the two orthogonal polarizations. Thus, a DP-BPSK signal can be phase regenerated with this scheme. This also means that phase fluctuations will be converted into amplitude fluctuations when operating in the small-signal regime. Operation in saturation will limit the amplitude fluctuation. Thus, simultaneous phase and amplitude regeneration can be achieved. In such a case, it is desired that the polarization channels of the DP-BPSK signal correspond to the $'x'$ and the $'y'$ polarizations. If the polarization channels correspond to any other linear polarization state, the amplitude of the $'x'$ and $'y'$ components does depend on the modulation symbol. Then, the polarization-diverse PSA when operating in saturation will distort the modulated signal unless the polarization channels correspond to the $'x'$ and the $'y'$ polarizations.

4.4 Non-Degenerate Vector Phase-Sensitive Amplification

The non-degenerate vector PSA was already analyzed in Section 3.3. In that section, we limited our analysis to the case of the signal being co-polarized with P_1, and the idler being orthogonal to the signal; and thus we described the input-output relations by scalar equations. However, the analysis can be extended to the case of arbitrary signal and idler input SOPs by using Jones vectors. The output signal, S_{out}, and the output idler I_{out} are the given by [90]

$$S_{\text{out}} = \mu S_{\text{in}} + \sigma\nu I_{\text{in}}^{*} \tag{4.13}$$

$$I_{\text{out}} = \mu I_{\text{in}} + \sigma\nu S_{\text{in}}^{*}, \tag{4.14}$$

where S_{in} and I_{in} are the input signal and idler Jones vectors, and

$$\sigma = \begin{bmatrix} 0 & 1 \\ 1 & 0 \end{bmatrix}. \tag{4.15}$$

The pump polarizations correspond to the $'x'$ and $'y'$ polarizations, meaning that we are defining the signal and idler SOPs with respect to the pump SOPs. We also assume phase-matching condition and pump phases such that μ and ν are real.

Following the definitions of signal and idler presented in Eqs. 4.4 and 4.5, the

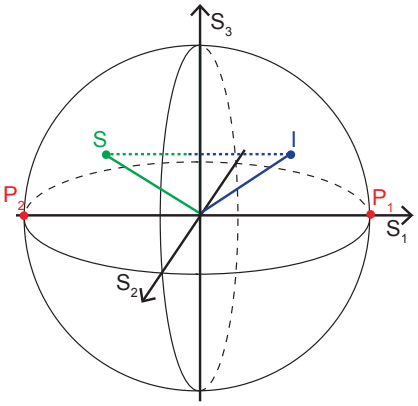

Figure 4.3: Relation between signal and idler SOPs to achieve maximum PS interaction in non-degenerate vector PSAs. The idler SOP is a mirror of the signal SOP the mirror plane defined by $S_1 = 0$.

gain is given by

$$\begin{aligned} G =& \frac{|S_{\text{out}}|^2}{|S_{\text{in}}|^2} = |\mu|^2 + |\nu|^2 \\ &+2|\mu||\nu|[\cos(\theta_{\text{S}})\sin(\theta_{\text{I}})\cos(\phi_{\text{S}} + \phi_{\text{I}} + \varphi_{\text{S}}/2 - \varphi_{\text{I}}/2) \\ &+\sin(\theta_{\text{S}})\cos(\theta_{\text{I}})\cos(\phi_{\text{S}} + \phi_{\text{I}} - \varphi_{\text{S}}/2 + \varphi_{\text{I}}/2)]. \end{aligned} \tag{4.16}$$

We can observe that maximum amplification can only be achieved when the signal and idler SOPs fulfill $\theta_{\text{S}} = \pi/2 - \theta_{\text{I}}$ and $\varphi_{\text{S}} = \varphi_{\text{I}}$, and the idler is a conjugated copy of the signal, $\phi_{\text{S}} = -\phi_{\text{I}}$. Using the conversion between Jones vector and Stokes vector presented in the Appendix, we can observe that maximum PS amplification is achieved when the idler polarization (described with Stokes parameters) fulfills

$$I_{\text{in}} = \begin{bmatrix} I_1 \\ I_2 \\ I_3 \end{bmatrix} = \begin{bmatrix} -S_1 \\ S_2 \\ S_3 \end{bmatrix}, \tag{4.17}$$

which means that the signal and idler SOPs should be mirrored in the $S_1 = 0$ plane as shown in Figure 4.3. If the signal and idler are orthogonally polarized and form a 45° angle with the pumps, $\theta_{\text{S}} = \theta_{\text{I}} = \pi/4$ and $\varphi_{\text{S}} = \varphi_{\text{I}}$, maximum PS amplification is achieved giving an the idler which is a conjugated copy of the signal, $\phi_{\text{S}} = -\phi_{\text{I}}$. If the signal and the idler are cross-polarized, maximum amplification occurs when they have the same polarization as the pumps as discussed in Section 3.3. On the contrary, if the signal and the idler are co-polarized with each other and with the pumps, $\theta_{\text{S}} = \theta_{\text{I}} = 0$, PS interaction is not achieved. Nor does PS interaction occur when they are cross-polarized with circular polarization. Thus, the gain of the amplifier is determined by the relative polarization between signal and idler as well as the absolute polarization. In the same way as in the polarization-diverse

two-mode PSA, an idler fulfilling those conditions can be created by a vector PI-FOPA regardless the signal input polarization and phase. This would lead to a scheme capable of phase-sensitively amplifying DP-modulated signals. However, such a scheme requires control of the relative signal and idler SOPs after the mid-stage with regard to the pump SOPs.

Comparing with the polarization-diverse PSA, both schemes provide the same gain for the same pump powers assuming phase-matching in both cases. Two scalar PI-FOPA sharing pump power (as in the case of polarization diversity) has the same gain as a single vector PI-FOPA using all the pump power when assuming exponential gain regime.

4.5 Degenerate Vector Phase-Sensitive Amplification

In the case of degenerate vector PSAs, the output signal Jones vector, S_{out} is given by

$$S_{\text{out}} = \mu S_{\text{in}} + \sigma \nu S_{\text{in}}^{*}, \tag{4.18}$$

where S_{in} is the input signal. The Pauli matrix, σ, was defined in 4.15. Note here that the idler mode is the 'y' component of the signal and the signal mode defined in Section 3.3 is the 'x' component of the signal described using Jones vector.

Similar to the polarization-diverse one mode PSA, we can gain much insight by describing the gain as the function of the signal input phase, ϕ_{S}, and polarization, θ_{S} and φ_{S}. In this case the gain is given by

$$G = \frac{|S_{\text{out}}|^2}{|S_{\text{in}}|^2} = \\ |\mu|^2 + |\nu|^2 + 2|\mu||\nu|[\sin(2\theta_{\text{S}})\cos(2\phi_{\text{S}})]. \tag{4.19}$$

This equation was obtained in [Paper A] but with a polarization description in the Stokes space. We address the cases of PI and PS gain separately below.

4.5.1 Phase-Insensitive Gain

When the signal is co-polarized with either of the pumps, $\theta = 0$ rad, phase-sensitive interaction is not achieved. A conjugated copy of the signal is generated in the orthogonal polarization. The generation of such a conjugated copy at the same wavelength can be used to perform dispersion compensation [125]. In this case of PI operation, the output signal polarization depends on the input signal phase since we have

$$S_{\text{out,x}}/S_{\text{out,y}} = \frac{\mu}{\nu}\exp(2i\phi_{\text{S}}). \tag{4.20}$$

In other words, the relative phase between the Jones components of the output signal depends on the input signal phase. As expected, their magnitude relation is independent of the signal phase. This property has been exploited in low power phase-sensitive processors. Since the polarization depends on the signal input phase, by placing a polarizer after the degenerate vector FOPA, phase-to-amplitude conversion can be achieved by the means of a PI-FOPA and a polarizer. Following [Paper C], if the polarizer is aligned to, e.g., the polarization defined by $\frac{1}{|\mu|^2+|\nu|^2}\begin{bmatrix}\nu\\ \mu\end{bmatrix}$, the signal after the polarizer has an amplitude that depends proportionally on the signal input in-phase component. Moreover, the phase of the signal after the polarizer can only take two values, i.e., the phase of the signal after this polarizer is squeezed. This scheme, degenerate vector PI-FOPA followed by a polarizer, can therefore be exploited to achieve phase quantizers with low pump powers [126]. In such a case, phase variations are converted into amplitude fluctuations unless the FOPA is operated in saturation. This limits the advantage of efficient phase regeneration at low pump powers. When operating at low gain, to obtain both quadratures, the signal after the degenerate vector PI-FOPA should be split into two branches with a polarizer in each branch selecting the corresponding signal quadratures. In the case of high-gain amplification $|\mu| \sim |\nu|$, both quadratures are demultiplexed into two cross-polarized components. Quadrature demultiplexing can then be achieved by the means of a PBS after the high-gain FOPA [Paper C].

4.5.2 Phase-Sensitive Gain

When the signal power is equally divided between both Jones components, $\theta_{\mathrm{S}} = 45°$, angle between the signal and the pumps, maximum PS interaction occurs. The gain is given by the same equation as in the polarization-diverse one-mode scalar PSA when operating in the PS-gain regime (Eq. 4.11). The relation between the signal output components is given by

$$S_{\mathrm{out,x}}/S_{\mathrm{out,y}} = \exp(i\varphi_{\mathrm{S}}), \tag{4.21}$$

which is the same relation as between the input components. Then, the signal polarization is not modified by the amplifier in this case.

In order to achieve PS gain, the signal Jones components need to be conjugated copies of each other. For instance, if the $'x'$ components is a QPSK signal, the 'y' components should be its conjugated copy. Such pair of conjugated and cross-polarized waves at the same wavelength can be achieved by means of a degenerate vector FOPA operating in PI mode. The copier is not required to generate such a pair of waves since any pair of two data signals which are cross-polarized and conjugated can be defined as a DP-ASK signal. The scheme also provides phase-squeezing for such signals [Paper B]. In the small-signal regime, both polarization channels can be phase-regenerated without cross-talk. In such a case, phase

fluctuations are converted into amplitude fluctuations. Considering the case of a DP-BPSK signal, saturation could be desired to avoid such amplitude fluctuations. However, crosstalk between the polarization channels appears when operating in saturation [90].

4.6 Practical Comparison

In this chapter, we have analyzed polarization-diverse and vector PSAs. Both signal-degenerate and non-degenerate cases have shown similar theoretical results. Assuming phase matching, both schemes provide the same gain for the same pump power. Also, the NF of the two cases is theoretically the same.

A copier-PSA scheme can be implemented in both cases providing a scheme which is WDM compatible, modulation-format independent and capable of operating with DP signals. However, different practical issues should be taken into account in this comparison. Vector PI-FOPAs [51] have shown worse NF than scalar PI-FOPA [99]. This degradation in vector FOPAs is usually attributed to the PMD in the HNLF. As discussed, polarization-diverse PI-FOPAs are penalized when using the same nonlinear medium. Mitigation of the penalties from reflections requires the uses of two-nonlinear media, which adds complexity to the scheme. The insertion loss of the PBS also degrades the performance of polarization-diverse PSAs. A major difference between both schemes is that the non-degenerate signal vector PSA requires two pumps while signal non-degenerate scalar PSA can be implemented with a single pump. The need for two pumps in the vector case is a drawback since it will add complexity to the pump recovery stage, which is necessary in the case of PS amplification after transmission as discussed in Section 3.5.

Both polarization-diverse one-mode PSAs or degenerate vector PSAs can perform phase-regeneration of DP-BPSK signals. When performing only phase regeneration the vector scheme is simpler and can provide similar performance as in that case the pump spacing does not need to be large. However, in most cases, operation in saturation is desired to remove amplitude fluctuations. In such situations, the vector PSA suffers from cross-talk between the polarization channels which will not be the case in the polarization-diverse PSA when the polarization channels are aligned to each PSA. Another difference between these schemes is that the scalar scheme suffers more from FWM between the pumps [Paper A], which can deplete the pumps.

Chapter 5
Conclusion and Future Outlook

Some of the most intriguing functionalities that PSAs can provide are low-noise amplification, cancellation of distortion induced by fiber nonlinearities and regeneration. Experimental demonstrations covering all these application have demonstrated the potential of PSAs. However, most demonstrations have been performed with signals modulated in one polarization. In order to demonstrate the full potential of PSAs, these demonstrations should also be performed with DP-modulated signals since future networks are expected to encode data on both polarizations. In such a scenario two PSA schemes capable of operating with DP signals arise: polarization diverse PSAs and vector PSAs. In this thesis, we have characterized the latter scheme, vector PSAs, and we have demonstrated that they are capable of providing both phase-regeneration and low-noise amplification. In our discussion, we have theoretically compared the two possible solutions and we have also discussed the practical differences between both solutions. This analysis should be complemented with experimental verification to provide a full understanding of the advantages provided by each scheme.

Regarding the regeneration applications, we have demonstrated that a degenerate vector PSA can phase regenerate both polarization channels of DP-BPSK [Paper B]. In order to make this scheme attractive for future networks, a black-box implementation should be demonstrated. Such a black-box implementation can be achieved by performing modulation stripping before the degenerate vector PSA. The crosstalk between polarization channels when operating in saturation should also be addressed. Numerical work has shown that vector PSAs are also capable of achieving phase-regeneration of DP-QPSK signals [127]. However, neither black-box implementation nor operation in saturation was discussed in that work.

The copier-PSA implementation is also feasible using either polarization-diverse or vector PSAs, which leads to WDM-compatible modulation-format independent PSA. Then, low-noise amplification and compensation of fiber nonlinearities can be achieved with both implementations. Experimental demonstration should confirm the potential of both schemes. A important aspect to overcome is that the copier-PSA implementation in both cases requires control of the global signal and idler

SOPs. In order to overcome that issue, two PLLs can be used when amplifying SP-modulated signals and using the polarization-diverse scheme [122]. However, that solution has not been demonstrated with DP-modulated signals. There is still need for demonstrations which show that PSA can operate in out-of-lab conditions with DP-modulated signals and transmission links. Up to know, all PSA in transmission links have been possible due to being in lab-conditions.

This evaluation of PSAs capable of amplifying DP signals should be extended to link transmission and be benchmarked by comparison to EDFA systems and Raman systems. In terms of noise, PSAs outperforms lumped PIAs . However, effective negative noise figure can be achieved with distributed amplifications such as Raman amplifiers. Parametric amplification has been demonstrated in distributed scenario using dispersion-shifted fiber (DSF) [128, 129], but such implementation is quite challenging in practical terms. Discussed theoretical [130,131], distributed PSAs is impractical and no demonstrations have been shown yet. Combination of Raman amplification and PSAs is an option whose consequences have not been experimentally evaluated. In such a scheme, the use of PSAs are expected to only double the distance in the linear regime at the expense of halving the spectral efficiency.

PSAs also perform all-optical compensation of fiber non-linearities, though not demonstrated yet with DP-modulated signals. PSAs can provide periodic compensation of fiber nonlinearities which is not possible when performing digital compensation. This opens the question of whether nonlinearities should be compensated periodically or at the receiver. The twin-wave approach must also be compared to other techniques which compensate for fiber non-linearities such as phase-conjugation and digital back-propagation.

Focusing on the vector schemes, an important aspect that that needs to be overcome is the performance degradation which is attributed to fiber PMD. The use of polarization-maintaining HNLF could mitigate such effect but a different model than the used in this thesis should be considered. For example, the gain when using polarization-maintaining-HNLF would be lower than in the case of using fiber with random birefringence. The use of vector PSAs can also bring new applications or provide better properties than scalar scheme. For instance, we demonstrated that both quadratures can be demultiplexed into two cross-polarized waves at the same wavelength as the input signal [Paper C]. Contrary to previous demonstrations of quadrature demultiplexing, both quadratures where obtained simultaneously [Paper C]. Therefore, research on vector PSA should be consider newer applications, including those outside of the telecom area.

Chapter 6
Summary of Papers

This thesis includes three appended papers, which are summarized below.

Paper A: Experimental analysis of degenerate vector phase-sensitive amplification

In this paper, we characterize a degenerate vector phase-sensitive amplifier and compare it to a degenerate scalar phase-sensitive amplifier. We show that the degenerate vector PSA is affected by fiber PMD, but the pump SOPs can be optimized to mitigate such effects. Once the pump SOPs are optimized, we show that the theoretical predictions agrees with the experimental setup regarding the gain and PSER curves as a function of the polarization angle between the degenerate wave and the pumps. In the comparison with the scalar case, we showed that the vector scheme is less affected by pump-pump FWM and higher-order idlers.

Paper B: Phase-sensitive amplification and regeneration of dual-polarization BPSK without polarization diversity

In this paper, we demonstrate that the degenerate vector PSA can amplify DP-BPSK signals with less added noise than EDFAs. A 1 dB sensitivity improvement is measured with respect to EDFA-based amplification. No penalty was observed by the presence of two polarization channels. The phase-regeneration capabilities of the vector PSA are evaluated by inputting a phase-degraded signal into the amplifier. At the output, we observe that the signal phase is regenerated and that phase fluctuations are converted into amplitude fluctuations.

Paper C: Quadrature demultiplexing using a degenerate vector parametric amplifier

Here, we demonstrate quadrature decomposition of a QPSK signal into a DP-BPSK signal. The decomposition is achieved by the means of a degenerate vector amplifier operating in PI mode. The high gain of the amplifier enables the decomposition into two cross-polarized waves, which are split by a PBS. Stable decomposition is achieved by using a novel PLL scheme which minimizes the amplitude variations of the decomposed signals. Thanks to this PLL, bit-error rate (BER) curves can be measured and confirm that both quadratures can be obtained simultaneously.

References

[1] K. C. Kao and G. A. Hockham, "Dielectric-fibre surface waveguides for optical frequencies," *Proceedings of the Institution of Electrical Engineers*, vol. 113, no. 7, pp. 1151–1158, Jul. 1966.

[2] R. J. Mears, L. Reekie, I. M. Jauncey, and D. N. Payne, "Low-noise erbium-doped fibre amplifier operating at 1.54 μm," *Electronics Letters*, vol. 23, no. 19, pp. 1026–1028, Sep. 1987.

[3] S. Makovejs, C. Roberts, F. Palacios, H. B. Matthews, D. A. Lewis, D. T. Smith, P. G. Diehl, J. J. Johnson, J. D. Patterson, C. Towery, and S. Ten, "Record-low 0.1460 dB/km attenuation ultra-large Aeff optical fiber for submarine applications," in *Optical Fiber Communication Conference (OFC)*, Mar. 2015, paper Th5A.2.

[4] T. Saitoh and T. Mukai, "1.5 μm GaInAsP traveling-wave semiconductor laser amplifier," *IEEE Journal of Quantum Electronics*, vol. 23, no. 6, pp. 1010–1020, Jun. 1987.

[5] M. O'Mahony, "Semiconductor laser optical amplifiers for use in future fiber systems," *Journal of Lightwave Technology*, vol. 6, no. 4, pp. 531–544, Apr. 1988.

[6] M. Islam, "Raman amplifiers for telecommunications," *IEEE Journal of Selected Topics in Quantum Electronics*, vol. 8, no. 3, pp. 548–559, May. 2002.

[7] J. Bromage, "Raman amplification for fiber communications systems," *Journal of Lightwave Technology*, vol. 22, no. 1, pp. 79–93, Jan. 2004.

[8] J. Hansryd, P. A. Andrekson, M. Westlund, J. Li, and P. Hedekvist, "Fiber-based optical parametric amplifiers and their applications," *IEEE Journal of Selected Topics in Quantum Electronics*, vol. 8, no. 3, pp. 506–520, May 2002.

[9] J. M. Chavez Boggio, S. Moro, E. Myslivets, J. R. Windmiller, N. Alic, and S. Radic, "155-nm continuous-wave two-pump parametric amplification," *IEEE Photonics Technology Letters*, vol. 21, no. 10, pp. 612–614, May 2009.

[10] T. Torounidis, P. A. Andrekson, and B. E. Olsson, "Fiber-optical parametric amplifier with 70-dB gain," *IEEE Photonics Technology Letters*, vol. 18, no. 10, pp. 1194–1196, May 2006.

[11] C. M. Caves, "Quantum limits on noise in linear amplifiers," *Physical Review D*, vol. 26, pp. 1817–1839, Oct. 1982.

[12] J. A. Levenson, I. Abram, T. Rivera, P. Fayolle, J. C. Garreau, and P. Grangier, "Quantum optical cloning amplifier," *Physical Review Letters*, vol. 70, pp. 267–270, Jan. 1993.

[13] J. A. Levenson, I. Abram, T. Rivera, and P. Grangier, "Reduction of quantum noise in optical parametric amplification," *Journal of the Optical Society of America B*, vol. 10, no. 11, pp. 2233–2238, Nov. 1993.

[14] M. E. Marhic, C. H. Hsia, and J.-M. Jeong, "Optical amplification in a nonlinear fibre interferometer," *Electronics Letters*, vol. 27, no. 3, pp. 210–211, Jan. 1991.

[15] Z. Tong, C. Lundström, P. A. Andrekson, C. J. McKinstrie, M. Karlsson, D. J. Blessing, E. Tipsuwannakul, B. J. Puttnam, H. Toda, and L. Grüner-Nielsen, "Towards ultrasensitive optical links enabled by low-noise phase-sensitive amplifiers," *Nature Photonics*, vol. 5, no. 7, pp. 430–436, Jun. 2011.

[16] R. Tang, J. Lasri, P. S. Devgan, V. Grigoryan, P. Kumar, and M. Vasilyev, "Gain characteristics of a frequency nondegenerate phase-sensitive fiber-optic parametric amplifier with phase self-stabilized input," *Optics Express*, vol. 13, no. 26, pp. 10 483–10 493, Dec. 2005.

[17] R. Tang, P. S. Devgan, V. S. Grigoryan, P. Kumar, and M. Vasilyev, "In-line phase-sensitive amplification of multi-channel CW signals based on frequency nondegenerate four-wave-mixing in fiber," *Optics Express*, vol. 16, no. 12, pp. 9046–9053, Jun. 2008.

[18] Z. Tong, C. Lundström, E. Tipsuwannakul, M. Karlsson, and P. Andrekson, "Phase-sensitive amplified DWDM DQPSK signals using free-running lasers with 6-dB link SNR improvement over EDFA-based systems," in *36th European Conference and Exhibition on Optical Communication (ECOC)*, Sep. 2010, paper PDP1.3.

[19] B. Corcoran, S. L. I. Olsson, C. Lundström, M. Karlsson, and P. A. Andrekson, "Phase-sensitive optical pre-amplifier implemented in an 80km DQPSK link," in *Optical Fiber Communication Conference*. Optical Society of America, Mar. 2012, paper PDP5A.4.

[20] Z. Tong, C. J. McKinstrie, C. Lundström, M. Karlsson, and P. A. Andrekson, "Noise performance of optical fiber transmission links that use non-degenerate cascaded phase-sensitive amplifiers," *Optics Express*, vol. 18, no. 15, pp. 15 426–15 439, Jul. 2010.

[21] C. J. McKinstrie, M. Karlsson, and Z. Tong, "Field-quadrature and photon-number correlations produced by parametric processes," *Optics Express*, vol. 18, no. 19, pp. 19 792–19 823, Sep. 2010.

[22] S. L. I. Olsson, C. Lundström, M. Karlsson, and P. A. Andrekson, "Long-haul (3465 km) transmission of a 10 GBd QPSK signal with low noise

phase-sensitive in-line amplification," in *2014 European Conference on Optical Communication (ECOC)*, Sep. 2014, paper PD.2.2.

[23] S. L. I. Olsson, B. Corcoran, C. Lundström, T. A. Eriksson, M. Karlsson, and P. A. Andrekson, "Phase-sensitive amplified transmission links for improved sensitivity and nonlinearity tolerance," *Journal of Lightwave Technology*, vol. 33, no. 3, pp. 710–721, Feb. 2015.

[24] K. Croussore, C. Kim, and G. Li, "All-optical regeneration of differential phase-shift keying signalsbased on phase-sensitive amplification," *Optics Letters*, vol. 29, no. 20, pp. 2357–2359, Oct. 2004.

[25] K. Croussore, I. Kim, Y. Han, C. Kim, G. Li, and S. Radic, "Demonstration of phase-regeneration of DPSK signals based on phase-sensitive amplification," *Optics Express*, vol. 13, no. 11, pp. 3945–3950, May 2005.

[26] K. Croussore, I. Kim, C. Kim, Y. Han, and G. Li, "Phase-and-amplitude regeneration of differential phase-shift keyed signals using a phase-sensitive amplifier," *Optics Express*, vol. 14, no. 6, pp. 2085–2094, Mar. 2006.

[27] K. Croussore and G. Li, "Phase regeneration of NRZ-DPSK signals based on symmetric-pump phase-sensitive amplification," *IEEE Photonics Technology Letters*, vol. 19, no. 11, pp. 864–866, Jun. 2007.

[28] F. Parmigiani, R. Slavík, J. Kakande, C. Lundström, M. Sjödin, P. A. Andrekson, R. Weerasuriya, S. Sygletos, A. D. Ellis, L. Grüner-Nielsen, D. Jakobsen, S. Herstrm, R. Phelan, J. O'Gorman, A. Bogris, D. Syvridis, S. Dasgupta, P. Petropoulos, and D. J. Richardson, "All-optical phase regeneration of 40Gbit/s DPSK signals in a black-box phase sensitive amplifier," in *2010 Conference on (OFC/NFOEC) Optical Fiber Communication (OFC), collocated National Fiber Optic Engineers Conference*, Mar. 2010, paper PDPC3.

[29] T. Umeki, M. Asobe, H. Takara, Y. Miyamoto, and H. Takenouchi, "Multi-span transmission using phase and amplitude regeneration in PPLN-based PSA," *Optics Express*, vol. 21, no. 15, pp. 18 170–18 177, Jul. 2013.

[30] J. Kakande, R. Slavík, F. Parmigiani, A. Bogris, D. Syvridis, L. Grüner-Nielsen, R. Phelan, P. Petropoulos, and D. J. Richardson, "Multilevel quantization of optical phase in a novel coherent parametric mixer architecture," *Nature Photonics*, vol. 5, no. 12, pp. 748–752, Oct. 2011.

[31] F. Da Ros, K. Dalgaard, L. Lei, J. Xu, and C. Peucheret, "QPSK-to-2×BPSK wavelength and modulation format conversion through phase-sensitive four-wave mixing in a highly nonlinear optical fiber," *Optics Express*, vol. 21, no. 23, pp. 28 743–28 750, Nov. 2013.

[32] F. Da Ros, K. Dalgaard, Y. Fukuchi, J. Xu, M. Galili, and C. Peucheret, "Simultaneous QPSK-to-2×BPSK wavelength and modulation format conversion in PPLN," *IEEE Photon. Technol. Lett.*, vol. 26, no. 12, pp. 1207–1210, Jun. 2014.

[33] M. Gao, T. Kurosu, T. Inoue, and S. Namiki, "Low-penalty phase demultiplexing of QPSK signal by dual-pump phase sensitive amplifiers," in *39th European Conference and Exhibition on Optical Communication (ECOC)*, Sep. 2013, paper We.3.A.5.

[34] Z. Tong, A. O. J. Wiberg, E. Myslivets, B. P. P. Kuo, N. Alic, and S. Radic, "Broadband parametric multicasting via four-mode phase-sensitive interaction," *Optics Express*, vol. 20, no. 17, pp. 19 363–19 373, Aug. 2012.

[35] T. Umeki, O. Tadanaga, A. Takada, and M. Asobe, "Phase sensitive degenerate parametric amplification using directly-bonded PPLN ridge waveguides," *Optics Express*, vol. 19, no. 7, pp. 6326–6332, Mar. 2011.

[36] M. Asobe, T. Umeki, and O. Tadanaga, "Phase sensitive amplification with noise figure below the 3 dB quantum limit using CW pumped PPLN waveguide," *Optics Express*, vol. 20, no. 12, pp. 13 164–13 172, Jun. 2012.

[37] T. Umeki, O. Tadanaga, M. Asobe, Y. Miyamoto, and H. Takenouchi, "First demonstration of high-order QAM signal amplification in PPLN-based phase sensitive amplifier," *Optics Express*, vol. 22, no. 3, pp. 2473–2482, Feb. 2014.

[38] Y. Zhang, C. Husko, J. Schröder, S. Lefrancois, I. H. Rey, T. F. Krauss, and B. J. Eggleton, "Phase-sensitive amplification in silicon photonic crystal waveguides," *Optics Letters*, vol. 39, no. 2, pp. 363–366, Jan. 2014.

[39] F. D. Ros, D. Vukovic, A. Gajda, K. Dalgaard, L. Zimmermann, B. Tillack, M. Galili, K. Petermann, and C. Peucheret, "Phase regeneration of DPSK signals in a silicon waveguide with reverse-biased p-i-n junction," *Optics Express*, vol. 22, no. 5, pp. 5029–5036, Mar. 2014.

[40] R. Neo, J. Schröder, Y. Paquot, D.-Y. Choi, S. Madden, B. Luther-Davies, and B. J. Eggleton, "Phase-sensitive amplification of light in a χ(3) photonic chip using a dispersion engineered chalcogenide ridge waveguide," *Optics Express*, vol. 21, no. 7, pp. 7926–7933, Apr. 2013.

[41] M. A. Ettabib, L. Jones, J. Kakande, R. Slavík, F. Parmigiani, X. Feng, F. Poletti, G. M. Ponzo, J. Shi, M. N. Petrovich, W. H. Loh, P. Petropoulos, and D. J. Richardson, "Phase sensitive amplification in a highly nonlinear lead-silicate fiber," *Optics Express*, vol. 20, no. 2, pp. 1629–1634, Jan. 2012.

[42] M. A. Ettabib, F. Parmigiani, X. Feng, L. Jones, J. Kakande, R. Slavík, F. Poletti, G. M. Ponzo, J. Shi, M. N. Petrovich, W. H. Loh, P. Petropoulos, and D. J. Richardson, "Phase regeneration of DPSK signals in a highly nonlinear lead-silicate W-type fiber," *Optics Express*, vol. 20, no. 24, pp. 27 419–27 424, Nov. 2012.

[43] K. Croussore and G. Li, "Phase and amplitude regeneration of differential phase-shift keyed signals using phase-sensitive amplification," *IEEE Journal of Selected Topics in Quantum Electronics*, vol. 14, no. 3, pp. 648–658, May 2008.

[44] R. Slavík, F. Parmigiani, J. Kakande, C. Lundström, M. Sjödin, P. A. Andrekson, R. Weerasuriya, S. Sygletos, A. D. Ellis, and L. Grüner-Nielsen,

"All-optical phase and amplitude regenerator for next-generation telecommunications systems," *Nature Photonics*, vol. 4, no. 10, pp. 690–695, Sep. 2010.

[45] G. Agrawal, *Nonlinear Fiber Optics*, 5th ed., ser. Optics and Photonics. Elsevier Science, 2013.

[46] M. Karlsson, "Four-wave mixing in fibers with randomly varying zero-dispersion wavelength," *Journal of the Optical Society America B*, vol. 15, no. 8, pp. 2269–2275, Aug. 1998.

[47] P. Velanas, A. Bogris, and D. Syvridis, "Impact of dispersion fluctuations on the noise properties of fiber optic parametric amplifiers," *Journal of Lightwave Technology*, vol. 24, no. 5, pp. 2171–2178, May 2006.

[48] Z. Tong, C. Lundström, M. Karlsson, and P. A. Andrekson, "Impact of zero-dispersion-wavelength distributions on the noise figure nonreciprocity of a fiber parametric amplifier," *IEEE Photonics Technology Letters*, vol. 23, no. 6, pp. 365–367, Mar. 2011.

[49] C. D. Poole and R. E. Wagner, "Phenomenological approach to polarisation dispersion in long single-mode fibres," *Electronics Letters*, vol. 22, no. 19, pp. 1029–1030, Sep. 1986.

[50] P. O. Hedekvist, M. Karlsson, and P. A. Andrekson, "Polarization dependence and efficiency in a fiber four-wave mixing phase conjugator with orthogonal pump waves," *IEEE Photonics Technology Letters*, vol. 8, no. 6, pp. 776–778, Jun. 1996.

[51] P. Kylemark, J. Ren, S. Radic, C. J. McKinstrie, M. Karlsson, and P. A. Andrekson, "Noise in orthogonally pumped fiber-optical parametric amplifiers," *IEEE Photonics Technology Letters*, vol. 19, no. 2, pp. 88–90, Jan. 2007.

[52] R. W. Boyd, *Nonlinear Optics*, ser. Nonlinear Optics Series. Elsevier Science, 2008.

[53] P. K. A. Wai and C. R. Menyuk, "Polarization mode dispersion, decorrelation, and diffusion in optical fibers with randomly varying birefringence," *Journal of Lightwave Technology*, vol. 14, no. 2, pp. 148–157, Feb. 1996.

[54] D. Marcuse, C. R. Menyuk, and P. K. A. Wai, "Application of the Manakov-PMD equation to studies of signal propagation in optical fibers with randomly varying birefringence," *Journal of Lightwave Technology*, vol. 15, no. 9, pp. 1735–1746, Sep. 1997.

[55] S. V. Manakov, "On the theory of two-dimensional stationary self-focusing of electromagnetic waves," *Journal of Experimental and Theoretical Physics*, vol. 38, no. 2, pp. 248–253, Feb. 1974.

[56] C. J. McKinstrie, H. Kogelnik, and L. Schenato, "Four-wave mixing in a rapidly-spun fiber," *Optics Express*, vol. 14, no. 19, pp. 8516–8534, Sep. 2006.

[57] C. J. McKinstrie, H. Kogelnik, R. Jopson, S. Radic, and A. Kanaev, "Four-wave mixing in fibers with random birefringence," *Optics Express*, vol. 12, no. 10, pp. 2033–2055, May 2004.

[58] A. Hasegawa and F. Tappert, "Transmission of stationary nonlinear optical pulses in dispersive dielectric fibers. i. anomalous dispersion," *Applied Physics Letters*, vol. 23, no. 3, pp. 142–144, Aug. 1973.

[59] L. F. Mollenauer, R. H. Stolen, and J. P. Gordon, "Experimental observation of picosecond pulse narrowing and solitons in optical fibers," *Physical Review Letters*, vol. 45, pp. 1095–1098, Sep. 1980.

[60] M.-C. Ho, K. Uesaka, M. E. Marhic, Y. Akasaka, and L. G. Kazovsky, "200-nm-bandwidth fiber optical amplifier combining parametric and Raman gain," *Journal of Lightwave Technology*, vol. 19, no. 7, pp. 977–981, Jul. 2001.

[61] P. L. Voss, K. G. Köprülü, and P. Kumar, "Raman-noise-induced quantum limits for $\chi(3)$ nondegenerate phase-sensitive amplification and quadrature squeezing," *Journal of the Optical Society America B*, vol. 23, no. 4, pp. 598–610, Apr. 2006.

[62] Z. Tong, A. Bogris, C. Lundström, C. J. McKinstrie, M. Vasilyev, M. Karlsson, and P. A. Andrekson, "Modeling and measurement of the noise figure of a cascaded non-degenerate phase-sensitive parametric amplifier," *Optics Express*, vol. 18, no. 14, pp. 14 820–14 835, Jul. 2010.

[63] R. Engelbrecht, "Analysis of SBS gain shaping and threshold increase by arbitrary strain distributions," *Journal of Lightwave Technology*, vol. 32, no. 9, pp. 1689–1700, May 2014.

[64] T. Nakanishi, M. Tanak, T. Hasegawa, M. Hirano, T. Okuno, and O. M., "Al_2O_3-SiO_2 core highly nonlinear dispersion-shifted fiber with brillouin gain suppression improved by 6.1 dB," in *2006 European Conference on Optical Communication (ECOC)*, Sep. 2006, paper Th.4.2.2.

[65] Y. Takushima and T. Okoshi, "Suppression of stimulated Brillouin scattering using optical isolators," *Electronics Letters*, vol. 28, no. 12, pp. 1155–1157, Jun. 1992.

[66] D. Cotter, "Suppression of stimulated Brillouin scattering during transmission of high-power narrowband laser light in monomode fibre," *Electronics Letters*, vol. 18, no. 15, pp. 638–640, Jul. 1982.

[67] J. Hansryd and P. A. Andrekson, "Broad-band continuous-wave-pumped fiber optical parametric amplifier with 49-dB gain and wavelength-conversion efficiency," *IEEE Photonics Technology Letters*, vol. 13, no. 3, pp. 194–196, Mar. 2001.

[68] A. Mussot, M. L. Parquier, and P. Szriftgiser, "Thermal noise for SBS suppression in fiber optical parametric amplifiers," *Optics Communications*, vol. 283, no. 12, pp. 2607 – 2610, 2010.

[69] M.-C. Ho, M. E. Marhic, K. Y. K. Wong, and L. G. Kazovsky, "Narrow-linewidth idler generation in fiber four-wave mixing and parametric amplification by dithering two pumps in opposition of phase," *Journal Lightwave Technology*, vol. 20, no. 3, pp. 469–476, Mar. 2002.

[70] J. Hansryd, F. Dross, M. Westlund, P. A. Andrekson, and S. N. Knudsen, "Increase of the SBS threshold in a short highly nonlinear fiber by applying a temperature distribution," *Journal of Lightwave Technology*, vol. 19, no. 11, pp. 1691–1697, Nov. 2001.

[71] M. R. Lorenzen, D. Noordegraaf, C. V. Nielsen, O. Odgaard, L. Grüner-Nielsen, and K. Rottwitt, "Suppression of Brillouin scattering in fibre-optical parametric amplifier by applying temperature control and phase modulation," *Electronics Letters*, vol. 45, no. 2, pp. 125–126, Jan. 2009.

[72] N. Yoshizawa and T. Imai, "Stimulated Brillouin scattering suppression by means of applying strain distribution to fiber with cabling," *Journal of Lightwave Technology*, vol. 11, no. 10, pp. 1518–1522, Oct. 1993.

[73] J. M. C. Boggio, J. D. Marconi, and H. L. Fragnito, "Experimental and numerical investigation of the SBS-threshold increase in an optical fiber by applying strain distributions," *Journal Lightwave Technology*, vol. 23, no. 11, pp. 3808–3814, Nov. 2005.

[74] M. Takahashi, M. Tadakuma, and T. Yagi, "Dispersion and Brillouin managed HNLFs by strain control techniques," *Journal Lightwave Technology*, vol. 28, no. 1, pp. 59–64, Jan. 2010.

[75] E. Myslivets, C. Lundström, J. M. Aparicio, S. Moro, A. O. J. Wiberg, C.-S. Bres, N. Alic, P. A. Andrekson, and S. Radic, "Spatial equalization of zero-dispersion wavelength profiles in nonlinear fibers," *IEEE Photonics Technology Letters*, vol. 21, no. 24, pp. 1807–1809, Dec. 2009.

[76] L. Grüner-Nielsen, S. Herstrøm, S. Dasgupta, D. J. Richardson, D. Jakobsen, C. Lundström, P. A. Andrekson, M. E. V. Pedersen, and B. Palsdottir, "Silica-based highly nonlinear fibers with a high SBS threshold," in *IEEE Winter Topicals Meetings (WTM)*, Jan. 2011, paper MD4.2.

[77] B. P.-P. Kuo, J. M. Fini, L. Grüner-Nielsen, and S. Radic, "Dispersion-stabilized highly-nonlinear fiber for wideband parametric mixer synthesis," *Optics Express*, vol. 20, no. 17, pp. 18 611–18 619, Aug. 2012.

[78] C. Lundström, R. Malik, L. Gruner-Nielsen, B. Corcoran, S. L. I. Olsson, M. Karlsson, and P. A. Andrekson, "Fiber optic parametric amplifier with 10-dB net gain without pump dithering," *IEEE Photon. Technol. Lett.*, vol. 25, no. 3, pp. 234–237, Feb. 2013.

[79] E. Mateo, F. Yaman, and G. Li, "Control of four-wave mixing phase-matching condition using the Brillouin slow-light effect in fibers," *Optics Letters*, vol. 33, no. 5, pp. 488–490, Mar. 2008.

[80] L. Wang and C. Shu, "Dynamic control of gain profile in fiber-optical parametric amplifier by gain-transparent SBS," *IEEE Photonics Technology Letters*, vol. 25, no. 20, pp. 1996–1999, Oct. 2013.

[81] ——, "Dynamic control of phase matching in four-wave mixing wavelength conversion of amplitude- and phase- modulated signals," *Journal of Lightwave Technology*, vol. 31, no. 9, pp. 1468–1474, May 2013.

[82] C. Huang, X. Guo, X. Fu, L. Wang, and C. Shu, "Active control of gain saturation in fiber-optical parametric amplifier using stimulated Brillouin scattering," *Optics Letters*, vol. 39, no. 19, pp. 5713–5716, Oct. 2014.

[83] C. J. McKinstrie and S. Radic, "Phase-sensitive amplification in a fiber," *Optics Express*, vol. 12, no. 20, pp. 4973–4979, Oct. 2004.

[84] C. J. McKinstrie, S. Radic, and M. Raymer, "Quantum noise properties of parametric amplifiers driven by two pump waves," *Optics Express*, vol. 12, no. 21, pp. 5037–5066, Oct. 2004.

[85] C. J. McKinstrie, S. Radic, and A. R. Chraplyvy, "Parametric amplifiers driven by two pump waves," *IEEE Journal of Selected Topics in Quantum Electronics*, vol. 8, no. 3, pp. 538–547, May 2002.

[86] Y. Chen and A. W. Snyder, "Four-photon parametric mixing in optical fibers: effect of pump depletion," *Optics Letters*, vol. 14, no. 1, pp. 87–89, Jan. 1989.

[87] W. Imajuku, A. Takada, and Y. Yamabayashi, "Inline coherent optical amplifier with noise figure lower than 3 dB quantum limit," *Electronics Letters*, vol. 36, no. 1, pp. 63–64, Jan. 2000.

[88] M. E. Marhic and C.-H. Hsia, "Optical amplification and squeezed-light generation in fibre interferometers performing degenerate four-wave mixing," *Quantum Optics*, vol. 3, no. 6, p. 341, Dec. 1991.

[89] C. J. McKinstrie, M. Yu, M. G. Raymer, and S. Radic, "Quantum noise properties of parametric processes," *Optics Express*, vol. 13, no. 13, pp. 4986–5012, Jun. 2005.

[90] M. E. Marhic, "Polarization independence and phase-sensitive parametric amplification," *Journal of the Optical Society of America B*, vol. 28, no. 11, pp. 2685–2689, Nov. 2011.

[91] J. Kakande, F. Parmigiani, M. Ibsen, P. Petropoulos, and D. J. Richardson, "Wide bandwidth experimental study of nondegenerate phase-sensitive amplifiers in single- and dual-pump configurations," *IEEE Photonics Technology Letters*, vol. 22, no. 24, pp. 1781–1783, Dec. 2010.

[92] T. Richter, B. Corcoran, S. L. Olsson, C. Lundström, M. Karlsson, C. Schubert, and P. A. Andrekson, "Experimental characterization of a phase-sensitive four-mode fiber-optic parametric amplifier," in *38th European Conference and Exhibition on Optical Communications (ECOC)*, Sep. 2012, paper Th.1.F.1.

[93] C. Lundström, Z. Tong, M. Karlsson, and P. A. Andrekson, "Phase-to-phase and phase-to-amplitude transfer characteristics of a nondegenerate-idler phase-sensitive amplifier," *Optics Letters*, vol. 36, no. 22, pp. 4356–4358, Nov. 2011.

[94] C. Lundström, B. Corcoran, M. Karlsson, and P. A. Andrekson, "Phase and amplitude characteristics of a phase-sensitive amplifier operating in gain saturation," *Optics Express*, vol. 20, no. 19, pp. 21 400–21 412, Sep. 2012.

[95] Y. Dai and C. Shu, "Bit-rate variable DPSK demodulation based on cascaded four-wave mixing," *Optics Express*, vol. 19, no. 4, pp. 2952–2958, Feb. 2011.

[96] X. Fu, Y. Dai, G. Lei, and C. Shu, "Bit-rate flexible demodulation of DPSK signals based on phase sensitive gain in cascaded four-wave mixing," *IEEE Photonics Technology Letters*, vol. 24, no. 12, pp. 994–996, Jun. 2012.

[97] R. Malik, A. Kumpera, A. Lorences-Riesgo, P. A. Andrekson, and M. Karlsson, "Frequency-resolved noise figure measurements of phase (in)sensitive fiber optical parametric amplifiers," *Optics Express*, vol. 22, no. 23, pp. 27 821–27 832, Nov. 2014.

[98] P. Kylemark, P.-O. Hedekvist, H. Sunnerud, M. Karlsson, and P. A. Andrekson, "Noise characteristics of fiber optical parametric amplifiers," *Journal of Lightwave Technology*, vol. 22, no. 2, pp. 409–416, Feb. 2004.

[99] Z. Tong, A. Bogris, M. Karlsson, and P. A. Andrekson, "Full characterization of the signal and idler noise figure spectra in single-pumped fiber optical parametric amplifiers," *Optics Express*, vol. 18, no. 3, pp. 2884–2893, Feb. 2010.

[100] Z. Tong, C. Lundström, M. Karlsson, M. Vasilyev, and P. A. Andrekson, "Noise performance of a frequency nondegenerate phase-sensitive amplifier with unequalized inputs," *Optics Letters*, vol. 36, no. 5, pp. 722–724, Mar. 2011.

[101] S. M. M. Friis, K. Rottwitt, and C. J. McKinstrie, "Raman and loss induced quantum noise in depleted fiber optical parametric amplifiers," *Optics Express*, vol. 21, no. 24, pp. 29 320–29 331, Dec. 2013.

[102] S. L. I. Olsson, B. Corcoran, C. Lundström, E. Tipsuwannakul, S. Sygletos, A. D. Ellis, Z. Tong, M. Karlsson, and P. A. Andrekson, "Injection locking-based pump recovery for phase-sensitive amplified links," *Optics Express*, vol. 21, no. 12, pp. 14 512–14 529, Jun. 2013.

[103] B. Corcoran, S. L. I. Olsson, C. Lundström, M. Karlsson, and P. A. Andrekson, "Mitigation of nonlinear impairments on QPSK data in phase-sensitive amplified links," in *39th European Conference and Exhibition on Optical Communication (ECOC)*, Sep. 2013, paper We.3.A.1.

[104] R. Slavík, A. Bogris, F. Parmigiani, J. Kakande, M. Westlund, M. Skoøld, L. Grüner-Nielsen, R. Phelan, D. Syvridis, P. Petropoulos, and D. J. Richardson, "Coherent all-optical phase and amplitude regenerator of binary phase-

encoded signals," *IEEE J. Sel. Top. Quantum Electron.*, vol. 18, no. 2, pp. 859–869, Mar. 2012.

[105] R. Slavík, A. Bogris, J. Kakande, F. Parmigiani, L. Grüner-Nielsen, R. Phelan, J. Vojtech, P. Petropoulos, D. Syvridis, and D. J. Richardson, "Field-trial of an all-optical PSK regenerator/multicaster in a 40 gbit/s, 38 channel DWDM transmission experiment," *Journal of Lightwave Technology*, vol. 30, no. 4, pp. 512–520, Feb. 2012.

[106] J. Kakande, A. Bogris, R. Slavík, F. Parmigiani, D. Syvridis, P. Petropoulos, and D. J. Richardson, "First demonstration of all-optical QPSK signal regeneration in a novel multi-format phase sensitive amplifier," in *36th European Conference and Exhibition on Optical Communication (ECOC)*, Sep. 2010, paper PD 3.3.

[107] J. Kakande, A. Bogris, R. Slavík, F. Parmigiani, D. Syvridis, M. Sköld, M. Westlund, P. Petropoulos, and D. J. Richardson, "QPSK phase and amplitude regeneration at 56 Gbaud in a novel idler-free non-degenerate phase sensitive amplifier," in *Optical Fiber Communication Conference/National Fiber Optic Engineers Conference*. Optical Society of America, Mar. 2011, p. OMT4.

[108] T. Richter, R. Elschner, and C. Schubert, "QAM phase-regeneration in a phase-sensitive fiber-amplifier," in *39th European Conference and Exhibition on Optical Communication (ECOC)*, Sep. 2013, paper We.3.A.2.

[109] A. Bogris, "All-optical demultiplexing of 16-QAM signals into QPSK tributaries using four-level optical phase quantizers," *Optics Letters*, vol. 39, no. 7, pp. 1775–1778, Apr. 2014.

[110] S. L. I. Olsson, T. A. Eriksson, C. Lundström, M. Karlsson, and P. A. Andrekson, "Linear and nonlinear transmission of 16-QAM over 105 km phase-sensitive amplified link," in *Optical Fiber Communication Conference (OFC)*, Mar. 2014, paper Th1H.3.

[111] X. Liu, A. R. Chraplyvy, P. J. Winzer, R. W. Tkach, and S. Chandrasekhar, "Phase-conjugated twin waves for communication beyond the Kerr nonlinearity limit," *Nature Photonics*, vol. 7, no. 7, pp. 560–568, May 2013.

[112] Y. Tian, Y.-K. Huang, S. Zhang, P. R. Prucnal, and T. Wang, "Demonstration of digital phase-sensitive boosting to extend signal reach for long-haul WDM systems using optical phase-conjugated copy," *Optics Express*, vol. 21, no. 4, pp. 5099–5106, Feb. 2013.

[113] X. Liu, H. Hu, S. Chandrasekhar, R. M. Jopson, A. H. Gnauck, M. Dinu, C. Xie, and P. J. Winzer, "Generation of 1.024-Tb/s Nyquist-WDM phase-conjugated twin vector waves by a polarization-insensitive optical parametric amplifier for fiber-nonlinearity-tolerant transmission," *Optics Express*, vol. 22, no. 6, pp. 6478–6485, Mar. 2014.

[114] H. Eliasson, S. L. I. Olsson, M. Karlsson, and P. A. Andrekson, "Comparison between coherent superposition in DSP and PSA for mitigation of

nonlinearities in a single-span link," in *2014 European Conference on Optical Communication (ECOC)*, Sep. 2014, paper Mo.3.5.2.

[115] T. Hasegawa, K. Inoue, and K. Oda, "Polarization independent frequency conversion by fiber four-wave mixing with a polarization diversity technique," *IEEE Photonics Technology Letters*, vol. 5, no. 8, pp. 947–949, Aug. 1993.

[116] K. K.-Y. Wong, M. E. Marhic, K. Uesaka, and L. G. Kazovsky, "Polarization-independent one-pump fiber-optical parametric amplifier," *IEEE Photonics Technology Letters*, vol. 14, no. 11, pp. 1506–1508, Nov. 2002.

[117] H. Hu, E. Palushani, M. Galili, H. C. H. Mulvad, A. Clausen, L. K. Oxenløwe, and P. Jeppesen, "640 Gbit/s and 1.28 Tbit/s polarisation insensitive all optical wavelength conversion," *Optics Express*, vol. 18, no. 10, pp. 9961–9966, May 2010.

[118] T. Richter, R. Elschner, A. Gandhe, K. Petermann, and C. Schubert, "Parametric amplification and wavelength conversion of single- and dual-polarization DQPSK signals," *IEEE Journal of Selected Topics in Quantum Electronics*, vol. 18, no. 2, pp. 988–995, Mar. 2012.

[119] R. M. Jopson and R. E. Tench, "Polarisation-independent phase conjugation of lightwave signals," *Electronic Letters*, vol. 29, pp. 2216–2217, Dec. 1993.

[120] K. Inoue, "Polarization independent wavelength conversion using fiber four-wave mixing with two orthogonal pump lights of different frequencies," *Journal Lightwave Technology*, vol. 12, no. 11, pp. 1916–1920, Nov. 1994.

[121] K. K.-Y. Wong, M. E. Marhic, K. Uesaka, and L. G. Kazovsky, "Polarization-independent two-pump fiber optical parametric amplifier," *IEEE Photonic Technology Letters*, vol. 14, no. 7, pp. 911–913, Jul. 2002.

[122] T. Umeki, T. Kazama, O. Tadanaga, K. Enbutsu, M. Asobe, Y. Miyamoto, and H. Takenouchi, "PDM signal amplification using PPLN-based polarization-independent phase-sensitive amplifier," *Journal of Lightwave Technology*, vol. 33, no. 7, pp. 1326–1332, Apr. 2015.

[123] G. K. P. Lei and M. E. Marhic, "Amplification of DWDM channels at 1.28 tb/s in a bidirectional fiber optical parametric amplifier," *Optics Express*, vol. 22, no. 7, pp. 8726–8733, Apr. 2014.

[124] M. E. Marhic, G. Kalogerakis, and L. G. Kazovsky, "Gain reciprocity in fibre optical parametric amplifiers," *Electronics Letters*, vol. 42, no. 9, pp. 519–520, Apr. 2006.

[125] B. P.-P. Kuo, E. Myslivets, A. O. J. Wiberg, S. Zlatanovic, C.-S. Brès, S. Moro, F. Gholami, A. Peric, N. Alic, and S. Radic, "Transmission of 640-Gb/s RZ-OOK channel over 100-km SSMF by wavelength-transparent conjugation," *Journal of Lightwave Technology*, vol. 29, no. 4, pp. 516–523, Feb. 2011.

[126] F. Parmigiani, G. Hesketh, R. Slavík, P. Horak, P. Petropoulos, and D. J. Richardson, "Optical phase quantizer based on phase sensitive four wave

mixing at low nonlinear phase shifts," *IEEE Photonics Technology Letters*, vol. 26, no. 21, pp. 2146–2149, Nov. 2014.

[127] W. Yang, Y. Yu, M. Ye, G. Chen, C. Zhang, and X. Zhang, "Phase regeneration for polarization-division multiplexed signals based on vector dual-pump nondegenerate phase sensitive amplification," *Optics Express*, vol. 23, no. 3, pp. 2010–2020, Feb. 2015.

[128] G. Kalogerakis, M. E. Marhic, K. K.-Y. Wong, and L. G. Kazovsky, "Transmission of optical communication signals by distributed parametric amplification," *J. Lightwave Technol.*, vol. 23, no. 10, p. 2945, Oct. 2005.

[129] X. Xu, C. Zhang, T. I. Yuk, and K. K. Y. Wong, "Distributed parametric amplifier for RZ-DPSK signal transmission system," *Optics Express*, vol. 20, no. 17, pp. 19 271–19 278, Aug. 2012.

[130] M. Vasilyev, "Distributed phase-sensitive amplification," *Optics Express*, vol. 13, no. 19, pp. 7563–7571, Sep. 2005.

[131] Z. Tong, C. Lundström, P. A. Andrekson, M. Karlsson, and A. Bogris, "Ultralow noise, broadband phase-sensitive optical amplifiers, and their applications," *IEEE Journal of Selected Topics in Quantum Electronics*, vol. 18, no. 2, pp. 1016–1032, Mar. 2012.

Appendix

A.1 Jones-Stokes Relation

The polarization of a wave with Jones description given by

$$E = \begin{bmatrix} E_{\mathrm{y}} \\ E_{\mathrm{y}} \end{bmatrix} = |E| e^{i\phi} \begin{bmatrix} \cos(\theta) e^{i\varphi/2} \\ \sin(\theta) e^{-i\varphi/2} \end{bmatrix} \tag{A.1}$$

is described by the Stokes vector

$$S = \begin{bmatrix} S_1 \\ S_2 \\ S_3 \end{bmatrix} = \begin{bmatrix} |E_{\mathrm{x}}|^2 - |E_{\mathrm{y}}|2 \\ 2Re(E_{\mathrm{x}} E_{\mathrm{y}}^*) \\ -2Im(E_{\mathrm{x}} E_{\mathrm{y}}^*) \end{bmatrix} = |E|^2 \begin{bmatrix} \cos(2\theta) \\ \sin(2\theta)\cos(\varphi) \\ -\sin(2\theta)\sin(\varphi) \end{bmatrix}, \tag{A.2}$$

from which it is clear that the conjugated Jones vector, E^*, has a Stokes vector with the opposite sign of the S_3 component.